



Calhoun: The NPS Institutional Archive
DSpace Repository

Theses and Dissertations

Thesis and Dissertation Collection

1994-03

Tropical cyclone development and
intensification under moderate to strong
vertical wind shear

Smith, Debra K.

Monterey, California. Naval Postgraduate School

<http://hdl.handle.net/10945/28618>

Downloaded from NPS Archive: Calhoun



Calhoun is a project of the Dudley Knox Library at NPS, furthering the precepts and goals of open government and government transparency. All information contained herein has been approved for release by the NPS Public Affairs Officer.

Dudley Knox Library / Naval Postgraduate School
411 Dyer Road / 1 University Circle
Monterey, California USA 93943

<http://www.nps.edu/library>

DUDLEY KNOX LIBRARY
NAVAL POSTGRADUATE SCHOOL
MONTEREY CA 93943-5101

Approved for public release; distribution is unlimited.

Tropical Cyclone Development and
Intensification Under Moderate to
Strong Vertical Wind Shear

by

Debra K. Smith
Lieutenant, United States Navy
B.S., University of Wisconsin Stevens Point, 1982

Submitted in partial fulfillment
of the requirements for the degree of

MASTER OF SCIENCE IN METEOROLOGY AND PHYSICAL
OCEANOGRAPHY

from the

NAVAL POSTGRADUATE SCHOOL
March 1994

REPORT DOCUMENTATION PAGE

Form Approved OMB No. 0704-0188

Public reporting burden for this collection of information is estimated to average 1 hour per response, including the time for reviewing instruction, searching existing data sources, gathering and maintaining the data needed, and completing and reviewing the collection of information. Send comments regarding this burden estimate or any other aspect of this collection of information, including suggestions for reducing this burden, to Washington Headquarters Services, Directorate for Information Operations and Reports, 1215 Jefferson Davis Highway, Suite 1204, Arlington, VA 22202-4302, and to the Office of Management and Budget, Paperwork Reduction Project (0704-0188) Washington DC 20503.

1. AGENCY USE ONLY (Leave blank)	2. REPORT DATE March 1994	3. REPORT TYPE AND DATES COVERED Master's Thesis	
4. TITLE AND SUBTITLE Tropical Cyclone Development and Intensification Under Moderate to Strong Vertical Wind Shear		5. FUNDING NUMBERS	
6. AUTHOR(S) Debra K. Smith			
7. PERFORMING ORGANIZATION NAME(S) AND ADDRESS(ES) Naval Postgraduate School Monterey CA 93943-5000		8. PERFORMING ORGANIZATION REPORT NUMBER	
9. SPONSORING/MONITORING AGENCY NAME(S) AND ADDRESS(ES)		10. SPONSORING/MONITORING AGENCY REPORT NUMBER	
11. SUPPLEMENTARY NOTES The views expressed in this thesis are those of the author and do not reflect the official policy or position of the Department of Defense or the U.S. Government.			
12a. DISTRIBUTION/AVAILABILITY STATEMENT Approved for public release; distribution is unlimited.		12b. DISTRIBUTION CODE A	
13. ABSTRACT (maximum 200 words) <p>A study was conducted to understand the physical mechanisms by which a tropical cyclone is able to develop and be maintained under moderate to strong vertical wind shear. The general approach was to describe case studies of three tropical cyclones in the western North Pacific that developed and/or intensified in the lee of another tropical cyclone. The data resources include high temporal and spatial resolution visible and infrared satellite imagery, operational subjective and objective analyses, plus special Tropical Cyclone Motion (TCM-90) high resolution (50 km) analyses and multi-quadric analyses.</p> <p>The three tropical cyclones developed and/or intensified under moderate to strong vertical wind shear that exceeded threshold values. The vertical wind shear was time dependent due to complex interactions with the leading tropical cyclone outflow, adjacent tropical upper tropospheric trough, and large-scale environment. Diurnal variability in strength of convection and outflow against the impinging flow led to fully exposed, partially exposed, or covered middle to lower tropospheric cyclonic circulation. Special characteristics of the monsoon trough circulation must create and sustain the tropical cyclone circulation against the tendency for the vertical wind shear to ventilate the vertical thermal and convective structure.</p>			
14. SUBJECT TERMS Tropical Cyclone, Vertical Wind Shear			15. NUMBER OF PAGES 119
			16. PRICE CODE
17. SECURITY CLASSIFICATION OF REPORT Unclassified	18. SECURITY CLASSIFICATION OF THIS PAGE Unclassified	19. SECURITY CLASSIFICATION OF ABSTRACT Unclassified	20. LIMITATION OF ABSTRACT UL

ABSTRACT

A study was conducted to understand the physical mechanisms by which a tropical cyclone is able to develop and be maintained under moderate to strong vertical wind shear. The general approach was to describe case studies of three tropical cyclones in the western North Pacific that developed and/or intensified in the lee of another tropical cyclone. The data resources include high temporal and spatial resolution visible and infrared satellite imagery, operational subjective and objective analyses, plus special Tropical Cyclone Motion (TCM-90) high resolution (50 km) analyses and multi-quadric analyses.

The three tropical cyclones developed and/or intensified under moderate to strong vertical wind shear that exceeded threshold values. The vertical wind shear was time dependent due to complex interactions with the leading tropical cyclone outflow, adjacent tropical upper tropospheric trough, and large-scale environment. Diurnal variability in strength of convection and outflow against the impinging flow led to fully exposed, partially exposed, or covered middle to lower tropospheric cyclonic circulation. Special characteristics of the monsoon trough circulation must create and sustain the tropical cyclone circulation against the tendency for the vertical wind shear to ventilate the vertical thermal and convective structure.

1 AC3
S 57596
C.1

TABLE OF CONTENTS

I. INTRODUCTION	1
II. BACKGROUND	4
A. TROPICAL CYCLOGENESIS	4
B. INTENSIFICATION	6
C. VERTICAL WIND SHEAR	8
III. DATA AND TOOLS	12
A. DATA SOURCES	12
1. OBJECTIVE ANALYSES	12
2. BEST TRACK DATA	13
3. SATELLITE IMAGERY	13
B. VERTICAL WIND SHEAR ANALYSIS	14
C. RELATIVE VORTICITY AND DIVERGENCE ANALYSIS	15
D. EFC ANALYSIS	15
IV. TROPICAL CYCLONE STEVE	17
A. TROPICAL DISTURBANCE STAGE (12 UTC 3 AUGUST TO 06 UTC 5 AUGUST)	17
B. TROPICAL DEPRESSION (TD) STAGE (12 UTC 5 AUGUST TO 00 UTC 7 AUGUST)	32
C. TROPICAL STORM (TS) STAGE (03 UTC 7 AUGUST TO 12 UTC 9 AUGUST)	41
D. SUMMARY	45

V. TROPICAL CYCLONE ZOLA	48
A. TROPICAL DISTURBANCE STAGE (06 UTC 15 AUGUST TO 00 UTC 17 AUGUST)	48
B. TROPICAL DEPRESSION STAGE (06 UTC 17 AUGUST TO 18 UTC 17 AUGUST)	59
C. TROPICAL STORM STAGE (00 UTC 18 AUGUST TO 00 UTC 19 AUGUST)	65
D. SUMMARY	69
VI. TROPICAL CYCLONE OMAR	72
A. TROPICAL DISTURBANCE STAGE (06 UTC 20 AUGUST TO 18 UTC 23 AUGUST)	72
B. TROPICAL DEPRESSION STAGE (00 UTC 24 AUGUST TO 18 UTC 24 AUGUST)	80
C. TROPICAL STORM STAGE (00 UTC 25 AUGUST TO 00 UTC 27 AUGUST)	84
D. TYPHOON STAGE (06 UTC 27 AUGUST TO 00 UTC 28 AUGUST)	90
E. SUMMARY	91
VII. CONCLUSIONS	93
A. SUMMARY AND DISCUSSION	93
B. FUTURE INVESTIGATIONS	97
LIST OF REFERENCES	99
INITIAL DISTRIBUTION LIST	103

LIST OF FIGURES

Figure 1. Two synoptic models of upper-level environmental flow patterns that are associated with enhanced tropical cyclone intensification (Sadler 1976). STR is SubTropical Ridge; SER is the SubEquatorial Ridge; and TUTT is the Tropical Upper Tropospheric Trough. 6

Figure 2. Plan views of zonal shear $U_{200 \text{ mb}} - U_{900 \text{ mb}}$ (m s^{-1}) for the Pacific data sets (McBride and Zehr 1981). N is for nondeveloping cases; and D is for the developing cases. 10

Figure 3. JTWC working best tracks for TC Robyn and TC Steve during August 1993. Positions at 6 h intervals are shown for the tropical disturbance/depression (circles), tropical storm (open cyclone symbols) and typhoon (closed cyclone symbols) stages. 18

Figure 4. Streamline analyses over the western North Pacific for 00 UTC 4 August 1993 at (a) 850 mb, and (b) 200 mb. 20

Figure 5. Vertical wind shear (m s^{-1}) between 200 mb and 850 mb over TC Steve (solid) for 12 UTC 3 August to 12 UTC 9

August 1993 calculated from the multi-quadric analyses, and over Guam (dashed) for 12 UTC 3 August to 00 UTC 8 August 1993 calculated from upper air soundings. 23

Figure 6. Low-level maximum velocity (intensity) of TC Steve (solid), 850/200 mb vertical wind shear (dot/dash), and translation speed (dashed) for 12 UTC 3 August to 12 UTC 9 August 1993. 24

Figure 7. 200 mb Eddy Flux Convergence (EFC) (contour interval $3 \text{ m s}^{-1} \text{ d}^{-1}$) from 12 UTC 3 August to 12 UTC 9 August 1993 for TC Steve calculated from the multi-quadric analyses. Solid (dashed) lines represent increasing (decreasing) cyclonic tendencies. 25

Figure 8. Relative vorticity (solid, 10^{-5} s^{-1}) and convergence (dashed, 10^{-5} s^{-1}) at 850 mb over TC Steve from 12 UTC 3 August to 12 UTC 9 August 1993 calculated from the multi-quadric analyses. 27

Figure 9. Visible satellite imagery at 0130 UTC 4 August 1993 showing the pre-Steve MCV (marked with 'x'). 28

Figure 10. Percentage of cloud tops in a 4 deg. lat. box centered on TC Steve with IR satellite imagery temperatures

less than -65°C (solid) and less than -85°C (dashed) for 12 UTC 3 August to 12 UTC 9 August 1993. 29

Figure 11. Minimum cloud top temperatures ($^{\circ}\text{C}$) for TC Steve (solid) and TC Robyn (dashed). Temperatures were obtained from IR satellite imagery each hour. 30

Figure 12. Schematic of Rossby wave train dispersion: (a) trough (C_T) of wave train generated by TC overlaps with anticyclone (A_G) of wave train generated by monsoon gyre; and (b) trough of wave train generated by TC does not overlap with wave train generated by monsoon gyre. 31

Figure 13. Streamline analyses over the western North Pacific for 00 UTC 7 August 1993 at (a) 850 mb, and (b) 200 mb. 33

Figure 14. (a) IR and (b) visible satellite imagery for 0030 UTC 6 August 1993 showing low-level cloudiness associated with 850 mb equatorial anticyclone. TD Steve is located in the upper right hand corner. 35

Figure 15. Enhanced IR satellite imagery for 1830 UTC 5 August 1993. Typhoon Robyn is located in upper left corner and TD Steve is located on right side. Cloud temperatures less than -65°C were enhanced. Notice the location of deep convection in

relation to the partially exposed low-level circulation of TD
Steve. 38

Figure 16. Visible satellite imagery for 0030 UTC 6 August
1993 showing the exposed LLCC of TD Steve. 39

Figure 17. Schematic of impinging upper-level flow causing (a)
subsidence within the center of the LLCC and convection
restricted to one side of the LLCC; (b) subsidence on the edge
of the LLCC with convection near the center and along one side
of the LLCC; and (c) fully covered LLCC with TC outflow
forcing descent outside of the system. 40

Figure 18. Streamline analyses over the western North Pacific
for 12 UTC 8 August 1993 at (a) 850 mb, and (b) 200 mb.
. 43

Figure 19. Streamline analyses over the western North Pacific
for 12 UTC 15 August 1990 at (a) 850 mb, and (b) 200 mb.
. 49

Figure 20. JTWC best tracks for TC Yancy and TC Zola during
August 1990 with symbols as in Fig. 3. 50

Figure 21. Relative vorticity (solid, 10^{-5} s^{-1}) and convergence
(dashed, 10^{-5} s^{-1}) at 850 mb over TC Zola from 12 UTC 15 August

to 00 UTC 19 August 1990 calculated from the TCM-90 analyses.

. 53

Figure 22. Vertical wind shear (m s^{-1}) over TC Zola from the TCM-90 analyses (solid) and over a ship (dashed) located between TC Zola and TC Yancy for 12 UTC 15 August to 00 UTC 19 August 1990 during each stage of TC Zola's development.

. 55

Figure 23. Low-level maximum velocity (intensity) of TC Zola (solid), 850/200 mb vertical wind shear (dot/dash), and translation speed (dashed) for 12 UTC 15 August to 00 UTC 19 August 1990. 56

Figure 24. 200 mb Eddy Flux Convergence (EFC) (contour interval $3 \text{ m s}^{-1} \text{ d}^{-1}$) from 12 UTC 15 August to 00 UTC 19 August 1990 for TC Zola calculated from the TCM-90 analyses. Solid (dashed) lines represent increasing (decreasing) cyclonic tendencies. 57

Figure 25. Streamline analyses over the western North Pacific for 18 UTC 17 August 1990 at (a) 850 mb, and (b) 200 mb.

. 60

Figure 26. IR satellite imagery for 1132 UTC 17 August 1990 showing the partial exposure of the LLCC for TD Zola with the

coldest cloud tops located over the southern edge of the LLCC.

. 64

Figure 27. IR satellite imagery for 1732 UTC 17 August 1990 showing the recovered LLCC of TD Zola with the coldest cloud tops located near the center and to the southwest portion of the LLCC. 65

Figure 28. Streamline analyses over the western North Pacific for 12 UTC 18 August 1990 at (a) 850 mb, and (b) 200 mb.

. 67

Figure 29. Visible satellite imagery for 0530 UTC 18 August 1990 showing the almost completely exposed LLCC of TS Zola.

. 69

Figure 30. JTWC best tracks for TC Omar and TC Polly during August 1992 with symbols as in Fig. 3. 73

Figure 31. Streamline analyses over the western North Pacific for 12 UTC 23 August 1992 at (a) surface/gradient level, and (b) 200 mb. 75

Figure 32. Vertical wind shear (m s^{-1}) over TC Omar from the multi-quadric analyses (solid) for 12 UTC 20 August 1990 to 00

UTC 28 August, and over Guam (dashed) for 12 UTC 24 August to 12 UTC 27 August 1992. 76

Figure 33. Low-level maximum velocity (intensity) of TC Omar (solid), 850/200 mb vertical wind shear (dot/dash), and translation speed (dashed) for 06 UTC 20 August to 00 UTC 28 August 1992. 77

Figure 34. 200 mb Eddy Flux Convergence (EFC) (contour interval $2 \text{ m s}^{-1} \text{ d}^{-1}$) from 12 UTC 20 August to 00 UTC 28 August 1992 for TC Omar calculated from the multi-quadric analyses. Solid (dashed) lines represent increasing (decreasing) cyclonic tendencies. 78

Figure 35. Minimum cloud top temperatures ($^{\circ}\text{C}$) from IR satellite imagery for TC Omar (solid) and TC Polly (dashed) for 0230 UTC 24 August to 1830 UTC 27 August 1992. 80

Figure 36. Relative vorticity (solid, 10^{-5} s^{-1}) and convergence (dashed, 10^{-5} s^{-1}) at 850 mb over TC Omar from 12 UTC 20 August to 00 UTC 28 August 1992 calculated from the multi-quadric analyses. 81

Figure 37. Streamline analyses over the western North Pacific for 12 UTC 24 August 1992 at (a) surface/gradient level, and

(b) 200 mb. 82

Figure 38. Streamline analyses over the western North Pacific for 12 UTC 26 August 1992 at (a) surface/gradient level, and

(b) 200 mb. 85

Figure 39. IR satellite imagery for 0330 UTC 25 August 1992 showing the outflow from TD Polly (left side) meeting the outflow from TS Omar (right side) over a relatively cloud-free area between the storms. 86

Figure 40. Visible satellite imagery for 0530 UTC 26 August showing the partially exposed mid-level vortex of TS Omar with the deepest convection located over the southwest portion of the vortex. 89

ACKNOWLEDGMENTS

I would like to thank Professor Russell Elsberry for his guidance, explanations, and patience. I could not have completed this thesis without his help. My thanks also go to Pat Harr and Jim Cowie for their assistance in learning to use the computer systems and software necessary to prepare the required data. I must also thank LCDR Les Carr and LT Rich Jeffries for their TCM-93 analyses.

I. INTRODUCTION

Tropical cyclogenesis is one of the least understood topics of tropical meteorology. This is due largely to the sparsity of observations within the tropics. Consequently, development and intensification of tropical cyclones (TC) are monitored and forecast primarily with satellite-based remote sensing techniques that are empirical.

The key to understanding tropical cyclogenesis is to explain the physical processes involved in various stages of the development from the convective disturbance or cloud cluster into a TC. A tropical disturbance is a cloud cluster that may or may not develop into a TC. A tropical depression is an area of organized convection with a closed cyclonic circulation that has maximum sustained winds of less than 17 m s^{-1} (34 kt). A tropical storm has maximum sustained winds between 17 and 32 m s^{-1} (35-64 kt). The generic term tropical cyclone will be used for all of these stages, and also include the hurricane (Atlantic and eastern North Pacific term) and typhoon (western North Pacific) stages.

For this study, the genesis stage is defined to be the transition of the tropical disturbance to a tropical storm, and intensification will refer to the transformation of a

tropical storm into a typhoon. Thus, tropical depressions are considered to still be undergoing cyclogenesis, while tropical storms have completed the genesis stage and are undergoing intensification.

It is generally accepted that small values of vertical wind shear are required for both genesis and intensification processes. Gray (1968) suggested that large values of vertical wind shear prevent the formation or maintenance of a warm core by advecting heat from the air column above the surface low pressure center. The decision trees of Simpson (1971) for operational prediction of development and intensification of TCs have as their first elements that the vertical wind shear between 200 and 850 mb must be less than 15 kt (7.7 m s^{-1}). Although McBride and Zehr (1981) state that favorable environmental conditions are zero shear over the developing system, large westerly zonal shear to the north and easterly zonal shear to the south are also favorable.

The focus of this paper is on the exceptions to the general "small vertical wind shear rules." This study will describe three cases in which moderate to strong vertical wind shear affected the development or intensification of a TC. The first two cases (TC Steve in 1993 and TC Zola in 1990) concern the development of a tropical disturbance in the wake of a large leading typhoon. These systems developed under moderate to strong vertical wind shear from the tropical disturbance stage to the tropical storm stage. The third case

(TC Omar in 1992) examines the delayed intensification of a tropical storm that came under vertical wind shear generated by a leading tropical storm embedded within a large monsoon gyre. Mechanisms that may have helped maintain the systems against the vertical wind shear will be discussed, and a preliminary conceptual model will be developed based on these case studies.

II. BACKGROUND

A. TROPICAL CYCLOGENESIS

Climatological studies show that about 80% of all tropical cyclones originate in or just poleward of the Inter-Tropical Convergence Zone (ITCZ) or monsoon trough (Gray 1968). The remaining TCs form in association with the Tropical Upper Tropospheric Trough (TUTT), waves in the easterly trade winds, and in baroclinic systems that penetrate into the tropics and are modified.

Although all theories require an initial disturbance, how the initial vortex forms from a pre-existing disturbance with deep convection is the topic of many hypotheses. Gray (1968, 1975, 1979) found that the climatological frequency of genesis was related to six favorable environmental factors: above-average low-level vorticity and middle-level moisture; conditional instability through a deep layer; a warm and deep oceanic mixed layer; weak vertical shear of the horizontal wind; and a location at least a few degrees poleward of the equator. As these conditions exist over much of the tropical oceans for long periods of time, it is not clear that these climatological factors are both necessary and sufficient conditions for tropical cyclogenesis.

In addition to these favorable factors, it is believed that some environmental forcing may be required. Wind surges are defined as low-level wind speed maxima typically appearing in the 850 mb analysis with an associated area of low-level mass convergence (Zehr 1992). One scenario is that a cold surge from the winter hemisphere raises pressure at the equator, which increases the zonal pressure gradient, and thus increases the southwesterly (in the Northern Hemisphere) winds into the monsoon trough. An intensification of the subtropical ridge may also lead to an increase in the easterlies on the poleward side of the monsoon trough. The low-level wind surge will increase the convergence within the monsoon trough, which can trigger deeper convection and possible TC development.

Cyclogenesis may also be triggered in the wake of another TC. Frank (1982) showed that TCs affect the circulation pattern within 1000-2000 km of the storm center in such a way as to enhance the potential for genesis of another storm in the wake and inhibit genesis ahead of the storm. According to Frank, this is due to the modification of the large-scale vertical velocity fields with ascent favored in the wake and descent ahead of the storm.

TCs initiated in association with cells in the TUTT are a summer feature of the central and western North Pacific (Sadler 1976). Although the surface system is initiated by the upper-level divergence to the east of the upper cell (Fig.

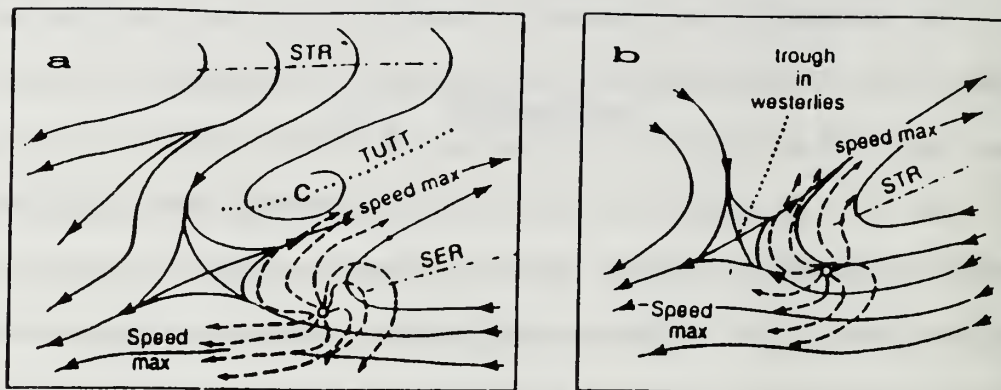


Figure 1. Two synoptic models of upper-level environmental flow patterns that are associated with enhanced tropical cyclone intensification (Sadler 1976). STR is SubTropical Ridge; SER is the SubEquatorial Ridge; and TUTT is the Tropical Upper Tropospheric Trough.

1a), the associated convection builds an upper tropospheric ridge or anticyclone that segments the TUTT and weakens or destroys the parent upper cell.

B. INTENSIFICATION

Due to the high inertial stability at low levels near the core of a mature TC, low-level environmental forcing plays a smaller role in the intensification stage of a TC. Charney and Eliassen (1964) and Ooyama (1963) proposed a linear stability theory, conditional instability of the second kind (CISK), which attributes TC intensification to an interaction between the convective and cyclone scales that is influenced by the surrounding environment. The CISK process involves frictional convergence of moisture by the large-scale circulation that enhances convection and increases latent heat

release, which then enhances the large-scale circulation. Thus, a feedback loop is established that maintains and intensifies the TC.

A second theory for intensification called the air-sea interaction theory has been proposed by Rotunno and Emanuel (1987) and Emanuel (1991). This theory is based on the hypothesis that the potential energy for TCs arises from the thermodynamic disequilibrium between the atmosphere and the underlying ocean. Because the transfer of latent and sensible heat from the ocean is a nonlinear function of surface wind speed, a stronger surface wind speed will increase these surface fluxes. The theory proposes that an increase in transfer of heat and moisture to the atmosphere associated with a finite-amplitude disturbance can lead to intensification of the TC.

Environmental forcing may play a role in TC intensification if it occurs in the upper troposphere where the inertial stability of the mature TC is at a minimum, which allows easier interaction between the TC and the surrounding environment. Sadler (1976, 1978) showed that when the TC moves to a position southeast of the TUTT cell (Fig. 1a), intensification of the TC may occur via enhancement of upper-level divergence and compensatory low-level convergence of heat and moisture. He suggested that the establishment of two outflow channels to the northeast into the midlatitudes and to

the southwest toward the equator is most favorable for rapid intensification.

As the TC moves poleward it comes under stronger westerly shear due to the strong midlatitude upper-tropospheric westerlies. This can lead to the shearing off of the upper-level warm core of the TC, which normally stops the intensification process. However, a midlatitude upper-level trough that approaches the TC (Fig. 1b) may lead to the establishment of an outflow channel to the westerlies (Chen and Gray 1986), which is favorable for intensification according to Sadler's model.

A sea-surface temperature (SST) greater than 26°C is considered to be a necessary condition for TC formation and intensification. Evans (1993) found that the local SST may provide an upper bound on TC intensity via a limit on energy available to the system. However, this limit does not appear to be the overriding factor restricting the development stage of TCs. Relating changes in TC intensity purely to changes in SST would be a vast oversimplification of the process.

C. VERTICAL WIND SHEAR

The warming of the air column by latent heat released during convection is important to the formation and intensification of the tropical cyclone. If net heating occurs in the column, the surface pressure will fall, which leads to the strengthening of the cyclonic circulation and

low-level inflow. As indicated in the Introduction, large values of vertical wind shear prevent this net accumulation from occurring, since the shear removes heat from the air column by a process called ventilation (Gray 1968). If the latent heat that is carried away is not replenished by low-level convergence and convection, the tropical disturbance will not develop.

A numerical study by Tuleya and Kurihara (1981) found that the degree of dynamic coupling between the low-level disturbance and upper-level flow is a prime indicator of subsequent genesis. In their numerical model, easterly vertical wind shear (easterly winds increasing with height) of moderate (10 m s^{-1}) magnitude is conducive for storm genesis, while westerly shear is detrimental to storm development.

As indicated above, a composite study by McBride and Zehr (1981) found a requirement for the existence of an east-west line of zero tropospheric zonal shear over the developing storm, with a large gradient of westerly shear to the north and easterly shear to the south (Fig. 2). Since the TC develops on the zero shear line, this appears to be a contradiction to the Tuleya and Kurihara numerical study in which moderate easterly shear over the TC did not inhibit genesis. The McBride and Zehr study also showed that the pattern of meridional shear is not important in the western Pacific. However, a composite of all developing storms in the Atlantic had a north-south line of zero vertical meridional

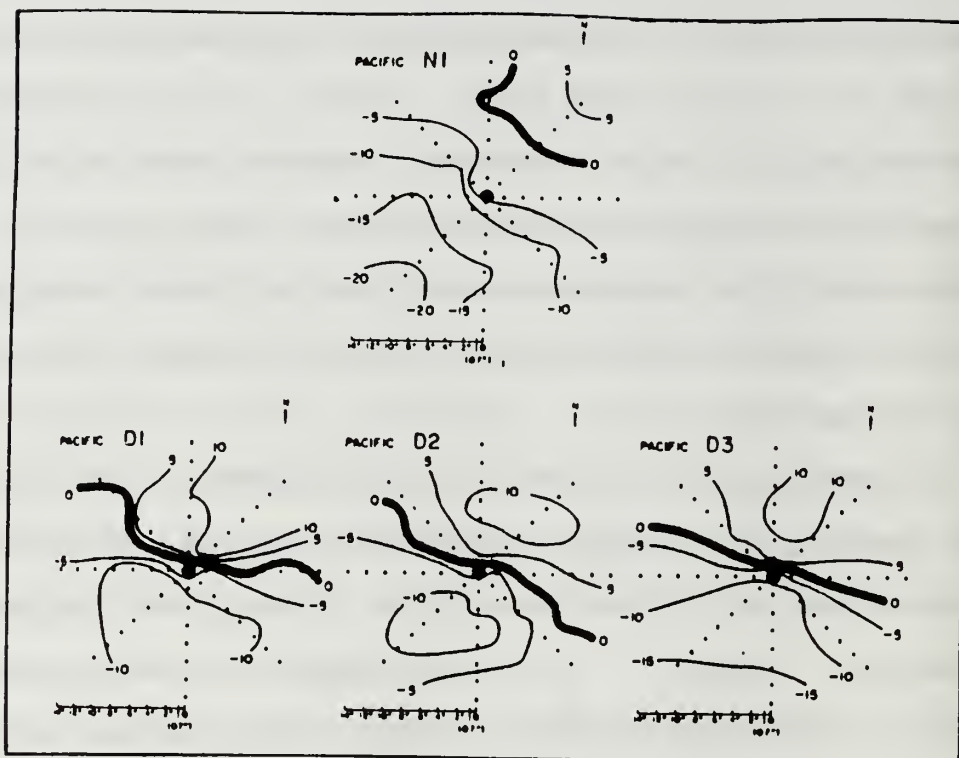


Figure 2. Plan views of zonal shear $U_{200 \text{ mb}} - U_{900 \text{ mb}}$ (m s^{-1}) for the Pacific data sets (McBride and Zehr 1981). N is for nondeveloping cases; and D is for the developing cases.

shear over the system center, with positive shear to the west and very strong negative shear to the east.

Two-dimensional modelling studies with specified upper-level momentum fluxes (Pfeffer and Challa 1981) and three-dimensional simulations with initial conditions from composite developing and nondeveloping tropical disturbance (Challa and Pfeffer 1990) indicate that upper-level eddy angular momentum fluxes (EFCs) can lead to tropical cyclone intensification. Molinari and Vollaro (1989, 1990) showed that upper-level eddy fluxes were important for the intensification of Hurricane Elena (1985). An observational study by DeMaria et al. (1993)

found that periods of enhanced EFC within 1500 km of the storm center tend to occur about every 5 days due to interactions with upper-level troughs in the midlatitude westerlies or with upper-level, cold lows in subtropical latitudes. Conflicting effects may occur as an adjacent trough becomes juxtaposed with the TC, since the EFC increases and so does the vertical wind shear. The regression analysis approach of DeMaria et al. indicates the contributions of SST and vertical wind shear are the leading elements in intensity changes of Atlantic TCs. Only after these two effects are considered do they find a correlation between EFC and intensity change. In the rapidly intensifying cases, the EFC was enhanced in six of ten cases, but the vertical shear remained low. These storms were located on the edge of the upper-level cyclonic features, which never moved directly over the TC. In most of their cases in which a period of enhanced EFC occurred but the storm did not intensify, the vertical shear increased, the storm moved over cold water, or the storm became extratropical.

In summary, it is generally accepted that weak vertical wind shear is a requirement for TC development. However, the following three case studies concern storms that developed under moderate to strong vertical wind shear.

III. DATA AND TOOLS

A. DATA SOURCES

1. Objective Analyses

Hand-drawn analyses by L. Carr III and R. Jeffries for 850 mb and 200 mb were used in determining the synoptic situation for TC Steve. Hand-drawn analyses from the staff of the Joint Typhoon Warning Center (JTWC) were available for the case study of TC Omar.

Analyses at 850 mb, 200 mb and sea-surface temperatures (SSTs) were obtained from Fleet Numerical Meteorology and Oceanography Center (FNMOC) for the TC Steve and TC Omar case studies. These analyses were created by the U.S. Navy Global Operational Atmospheric Prediction System (NOGAPS), which includes a full physics spectral model that is used for operational weather prediction. The archived analyses have a horizontal resolution of 2.5 degrees and were available at each 12 h. Hogan and Rosmond (1991) describe the NOGAPS analysis and forecast model in detail.

For the case study of TC Zola, high resolution analyses were produced for the Office of Naval Research Tropical Cyclone Motion (TCM) field experiment held August to September 1990. These TCM-90 final analyses were prepared by the U.S. National Meteorological Center (NMC) based on all the

real-time and delayed data from the experiment. A description of the observational systems that provided the data and data handling procedures is given in Elsberry et al. (1990). A multivariate objective analysis was used for the wind and mass fields. No bogus of the TC position or inner core structure was used to avoid contamination of outer wind structure that was resolved by observations. Analysis horizontal and vertical resolution are 50 km and 20 levels. The analyses were prepared each 6 h for the time of interest for TC Zola.

2. Best Track Data

The best track data for the TC Omar and TC Zola cases were obtained from JTWC. Best track positions are generated after the storm by subjectively constructing a smooth path through the individual storm fixes. At the time of this study, the best tracks were not available for TC Steve and its leading TC, TC Robyn. Only the working best tracks are available from JTWC for these 1993 storms. Working best tracks are the real-time updates of the storm track that were generated during the storm.

3. Satellite Imagery

High resolution satellite imagery was obtained from JTWC for the case studies of TC Steve and TC Omar. The Japanese Geostationary Meteorological Satellite (GMS) has a visible infrared spin scan radiometer (VISSR), for which the spatial resolution of the visual images is 1.25 km and of the

infrared (IR) images is 5 km (Rao et al. 1990). The temporal resolution is hourly for IR and visual (during daylight hours) imagery for TC Steve. Hourly temporal resolution from 2230 UTC 24 August 1992 to 1830 UTC 27 August 1992 is available for TC Omar. Unfortunately, the imagery is only available each 3 h earlier on 24 August and during the nighttime hours (0830-2030 UTC) on 23 August.

For the case study TC Zola, only hard copies of high resolution satellite imagery are available on a sporadic basis from 17 - 20 August 1990. Hard copies include visual, IR, and IR enhanced imagery.

B. VERTICAL WIND SHEAR ANALYSIS

Vertical wind shear is calculated from the 850 and 200 mb wind analyses using

$$|\Delta \vec{v}| = \sqrt{(u_{200} - u_{850})^2 + (v_{200} - v_{850})^2}.$$

A zonal vertical wind shear similar to McBride and Zehr (1981) is also defined as $\Delta u = u_{200} - u_{850}$. The best track position is used in conjunction with the shear charts to calculate the shear over the TC. The 50 km TCM-90 analyses are used to calculate the vertical wind shear for the TC Zola case.

Since the resolution of the NOGAPS charts is only 2.5 degrees (approximately 280 km), a multiquadric interpolation was used to improve the resolution. Application of the multiquadric interpolation theory to meteorological objective

analysis is described in detail by Nuss and Titley (1994). The two-dimensional, single-variable analysis procedure they describe resulted in high quality analyses that compared favorably to the Barnes and Cressman analysis techniques. For this study, a two-dimensional multiquadric interpolation program developed by D.W. Titley was used. The NOGAPS analyses were the first-guess field, and rawinsondes, satellite cloud-track winds, and aircraft reports were used to analyze 850 and 200 mb wind fields with 50 km resolution.

C. RELATIVE VORTICITY AND DIVERGENCE ANALYSIS

The relative vorticity is calculated as

$$\zeta_{(i,j)} = \frac{V_{(i+1,j)} - V_{(i-1,j)}}{2\Delta x} - \frac{U_{(i,j+1)} - U_{(i,j-1)}}{2\Delta y}.$$

Similarly, divergence is calculated as

$$D_{(i,j)} = \frac{U_{(i+1,j)} - U_{(i-1,j)}}{2\Delta x} + \frac{V_{(i,j+1)} - V_{(i,j-1)}}{2\Delta y}.$$

The 850 mb and 200 mb relative vorticity and divergence were computed on the 50 km grid. Values for the TC Zola case were calculated each 6 h, while for TC Steve and TC Omar the values were calculated each 12 h.

D. EFC ANALYSIS

The eddy flux convergence (EFC) of angular momentum is equal to

$$EFC = -\frac{1}{r^2} \frac{\partial}{\partial r} (r^2 \overline{u'v'}),$$

where r is the radius in cylindrical coordinates, u' and v' are the eddy radial and tangential wind components respectively, and an overbar indicates an azimuthal average. The EFC is calculated at 200 mb every 50 km from the storm center to 1500 km (units of $\text{m s}^{-1} \text{d}^{-1}$)

$$EFC_{j-1} = \frac{-[r_j^2 (\overline{v_{\theta_j} v_{r_j}}) - r_{j-1}^2 (\overline{v_{\theta_{j-1}} v_{r_{j-1}}})]}{r_{(j-\frac{1}{2})}^2 \Delta r}.$$

The EFC calculations are available each 12 h, except for TC Zola where they are available each 6 h.

IV. TROPICAL CYCLONE STEVE

A. TROPICAL DISTURBANCE STAGE (12 UTC 3 AUGUST TO 06 UTC 5 AUGUST)

The pre-Steve tropical disturbance was detected as a persistent area of convection to the east-southeast of Typhoon Robyn. It was a mesoscale convective system (MCS), which is defined as a precipitation system on spatial scales from 20 to 500 km that includes deep convection during some part of its lifetime (Hane 1986).

The tracks of Robyn and Steve are shown in Fig. 3. Due to the combined influence of the low-level circulation around Robyn and the monsoon trough, pre-Steve drifted north-northeast at about 4 kt until 06 UTC 4 August. The slow speed of movement may have been due to the diabatic contribution to storm propagation opposing the advective effect. That is, the location of the maximum latent heat release was occurring in the southern portion of the MCS where the deepest convection and the low-level moist inflow occurred. The separation distance between the two storms increased from 11.9 to 13.9 deg. of lat. during this time. From 06 UTC 4 August to the end of the tropical disturbance stage, pre-Steve tracked northwest at 5-8 kt in the southeasterly inflow to Typhoon Robyn. As Robyn also moved northwest during this period at 7-

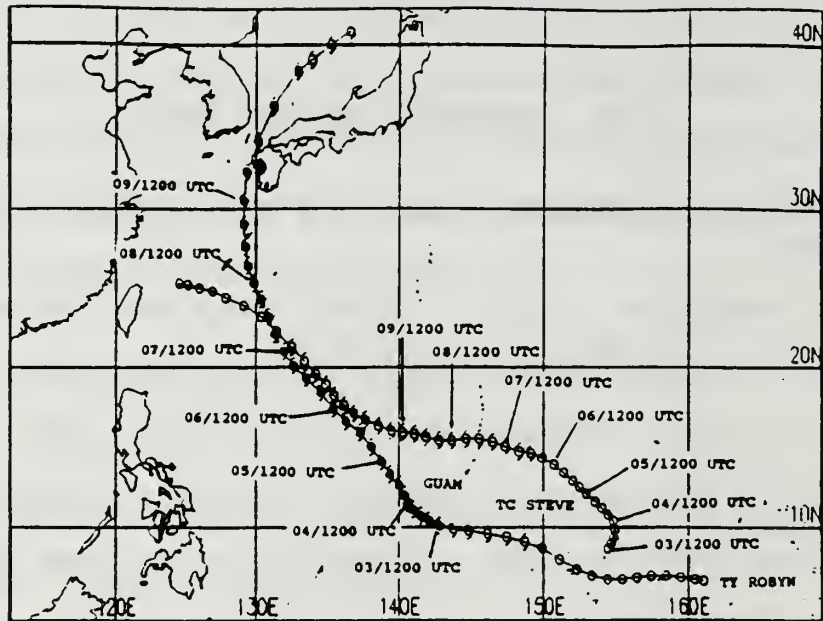


Figure 3. JTWC working best tracks for TC Robyn and TC Steve during August 1993. Positions at 6 h intervals are shown for the tropical disturbance/depression (circles), tropical storm (open cyclone symbols) and typhoon (closed cyclone symbols) stages.

12 kt, the separation distance between the two storms increased from 13.9 to 14.8 deg. lat.

Briegel (1993) studied 30 cases in which a TC formed when one or two TCs already existed. She concluded that a TC does not form until the pre-existing TC is on the average approximately 20 deg. long. (about 18 deg. lat.) to the west. The minimum separation distance was at least 10 deg. long. (9 deg. lat.) to the west. One hypothesis to be tested here is that a new storm cannot develop at smaller separation distances due to the strong vertical wind shear generated by the pre-existing TC. That is, the minimum separation distance is possibly dependent on how well developed the upper-level

outflow is for the pre-existing TC, and therefore how far eastward the strong vertical shear extends. Since Robyn's outflow (to be shown in Fig. 4b) was constricted on the eastern side, the MCS was possibly able to maintain its existence within 12 deg. lat. of Robyn.

The hand-drawn analyses for 850 mb and 200 mb were used to determine the synoptic conditions (and associated figures) for this case. Multi-quadric analyses were used to calculate the vertical wind shear, relative vorticity, and convergence. The best agreement between the hand-drawn analyses and the multi-quadric analyses was at 850 mb. At 850 mb, the location of centers and agreement in the overall flow were good. At 200 mb, the hand-drawn analyses appear to have more mesoscale features than the multi-quadric analyses. The agreement on synoptic features (i.e., the TUTT) was good and the flow over TC Steve throughout the case generally agreed in direction and magnitude.

The 00 UTC 4 August 850 mb analysis (Fig. 4a), is typical of the low-level synoptic conditions during this stage. Both Robyn and pre-Steve were located in the convergent, low-level monsoon trough. A surge from the southwest into the monsoon trough occurred from 12 UTC 3 August to 00 UTC 4 August. Although a 35 kt southwesterly wind was present at 850 mb in the inflow to Steve at Chuuk (7.5°N , 152.0°E), the inflow winds then decreased to 10 kt by 12 UTC 4 August. An area of low-level mass convergence was associated with the surge. Zehr

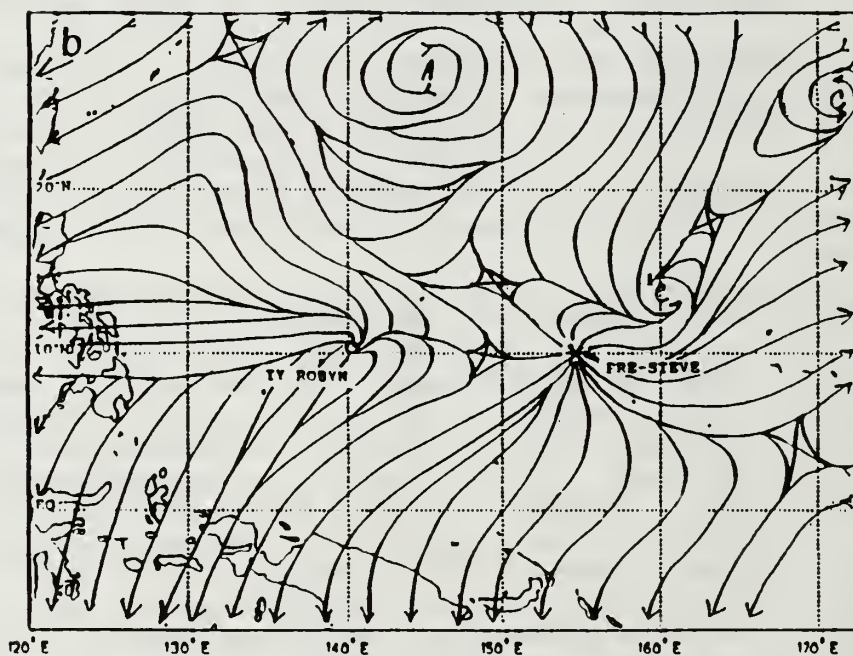
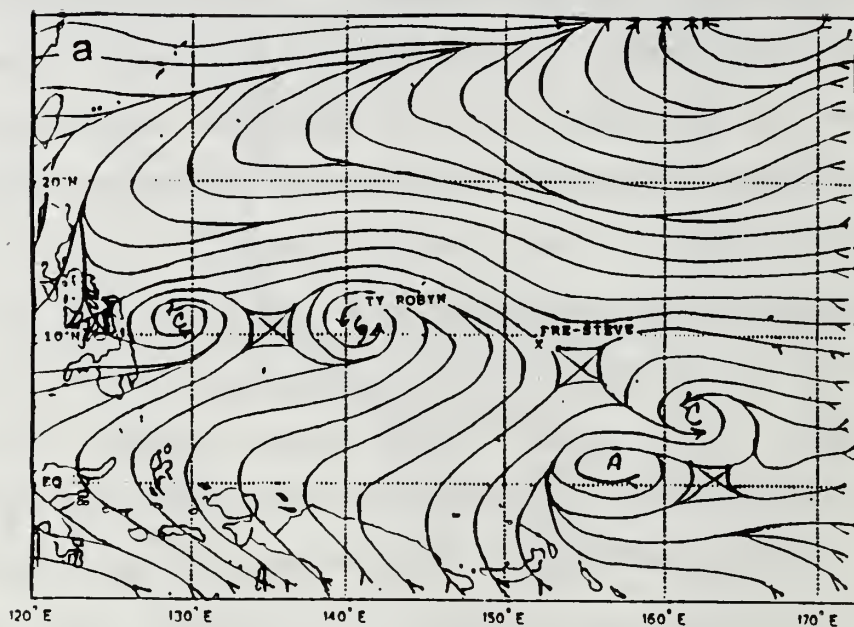


Figure 4. Streamline analyses over the western North Pacific for 00 UTC 4 August 1993 at (a) 850 mb, and (b) 200 mb.

(1992) proposes that the interaction of the surge with a tropical disturbance or depression will enhance the low-level convergence, which results in more deep convection. The pressure gradient between the subtropical ridge to the north of the system and the monsoon trough maintained 15-25 kt winds north of the disturbance. Soundings from two island stations, Chuuk to the southwest and Ponape (7.0° , 158.2° E) to the southeast, showed available moisture (dewpoint depression less than 5° C) from the surface to at least 400 mb. Based on the FNMOC SST analyses, the pre-Steve disturbance formed over water with a SST of 29° C, which exceeded the minimum for TC formation of 26.5° C (Frank 1987). The SST remained higher than the minimum throughout the entire case study.

Binary TC interaction may result in an increased counterclockwise rotation of two systems with similar intensities that are separated by less than 6 deg. lat. (Elsberry 1987). However, the environmental steering effect becomes progressively more important than the Fujiwhara effect when a separation distance of 7 to 15 deg. lat. exists between the two TCs. Based on Fig. 4a, this appears to be the situation for pre-Steve, in that the early portion of the storm track may be due to a combination of the environmental steering and the circulation of Robyn. The cyclonic curvature in pre-Steve's track (Fig. 3) throughout this disturbance stage evidently resulted from the influence of the circulation of Robyn. However, this may not be characterized as a binary

cyclone interaction (Fujiwhara effect) because the small circulation of pre-Steve did not noticeably affect Robyn's track.

The western edge of the TUTT was located north to northeast of the pre-Steve disturbance throughout the period (Fig. 4b). According to Sadler (1976), this location of the TUTT may have aided in the development of the pre-Steve disturbance by putting divergence over the system and also by providing an outflow channel to the westerlies, which can increase the evacuation of mass from the disturbance (Frank 1987). The small TUTT cell that was to the northeast of pre-Steve in Fig. 4b weakened and was no longer analyzed at 00 UTC 5 August (not shown). Although Typhoon Robyn maintained a nearly constant intensity during the period, its outflow was constricted on the eastern side (Fig. 4b) as it approached pre-Steve. Thus, the vertical shear over the pre-Steve disturbance during this early stage appears to be due to the upper-level divergent flow around the TUTT interacting with a point-source of divergence over pre-Steve.

The vertical wind shears over the TC Steve disturbance and over Guam are shown in Fig. 5. The island station of Guam was chosen due to its location between Typhoon Robyn and TC Steve through 12 UTC 7 August, as can be seen in Fig. 3. For the tropical disturbance stage, the vertical wind shear over the pre-Steve disturbance was generally less than the 12.5 m s^{-1} threshold for development specified by Zehr (1992). The

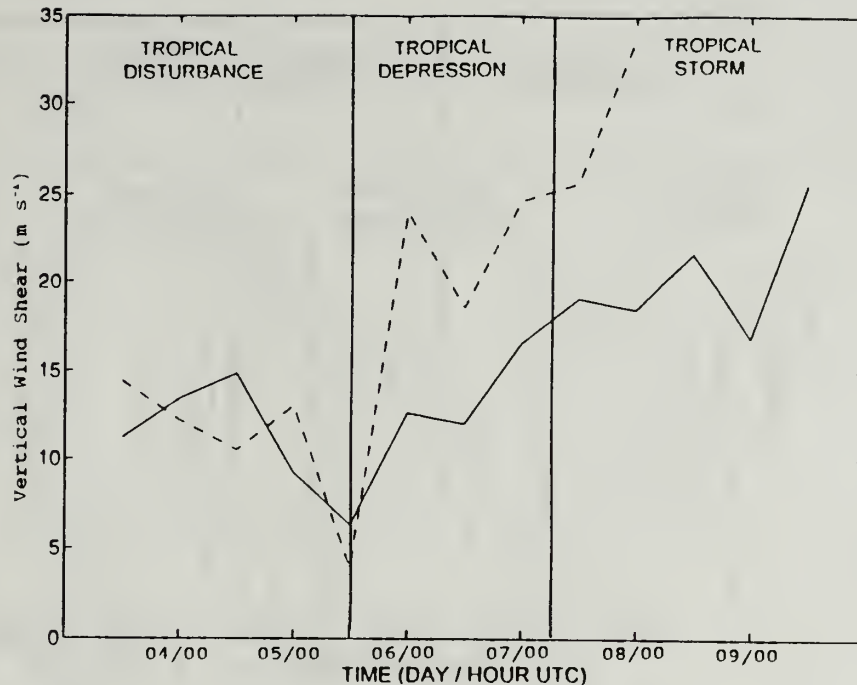


Figure 5. Vertical wind shear (m s^{-1}) between 200 mb and 850 mb over TC Steve (solid) for 12 UTC 3 August to 12 UTC 9 August 1993 calculated from the multi-quadric analyses, and over Guam (dashed) for 12 UTC 3 August to 00 UTC 8 August 1993 calculated from upper air soundings.

intensity of pre-Steve remained steady under the moderate vertical wind shear. As the shear magnitude decreased both over pre-Steve and over Guam at the end of this stage, the maximum wind velocity (intensity) of pre-Steve increased (Fig. 6). The minimum vertical wind shear magnitude corresponded to the development of pre-Steve into a tropical depression.

The eddy flux convergence (EFC) of angular momentum was generally positive (Fig. 7) during 18 UTC 3 August to 18 UTC 4 August from the storm center to 1500 km. However, a transient period of negative EFC within 400 km of pre-Steve occurred at 00 UTC 5 August. When the EFC is positive, the eddy fluxes are acting to make the upper-level flow more

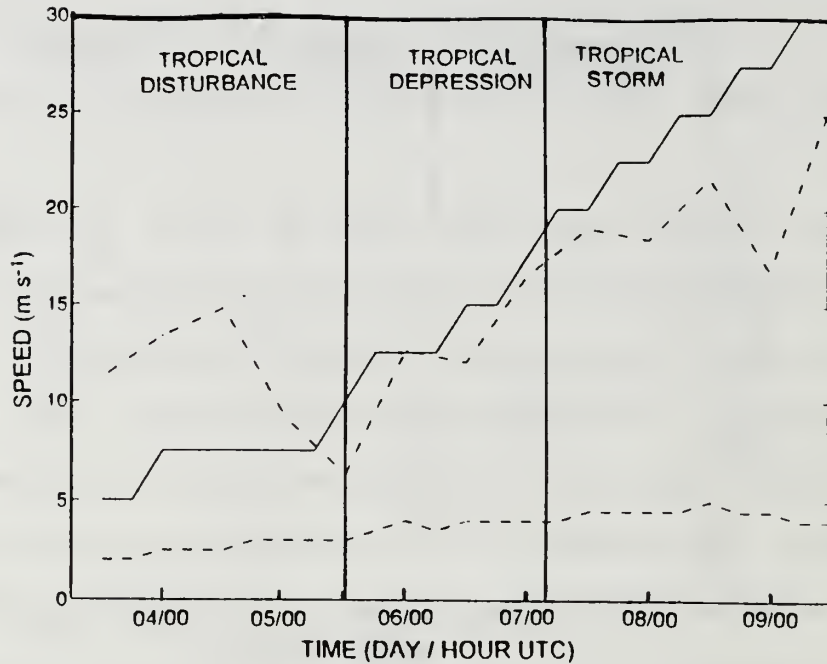


Figure 6. Low-level maximum velocity (intensity) of TC Steve (solid), 850/200 mb vertical wind shear (dot/dash), and translation speed (dashed) for 12 UTC 3 August to 12 UTC 9 August 1993.

cyclonic. If the EFC increases with height to a maximum in the upper troposphere, conditions are conducive for TC development according to DeMaria et al. (1993).

The pattern of zonal vertical wind shear (not shown) resembled the McBride and Zehr (1981) pattern in Fig. 2, except that pre-Steve is located under about $5\text{--}10 \text{ m s}^{-1}$ vertical wind shear. Zehr (1992) calculated threshold values for 850 mb relative vorticity and convergence during TC formations in the western North Pacific. Relative vorticity has a typical range of -2.5 to $2.5 \times 10^{-5} \text{ s}^{-1}$ and is generally expected to be greater than $1 \times 10^{-5} \text{ s}^{-1}$ for development to occur. Convergence values at 850 mb should have a magnitude

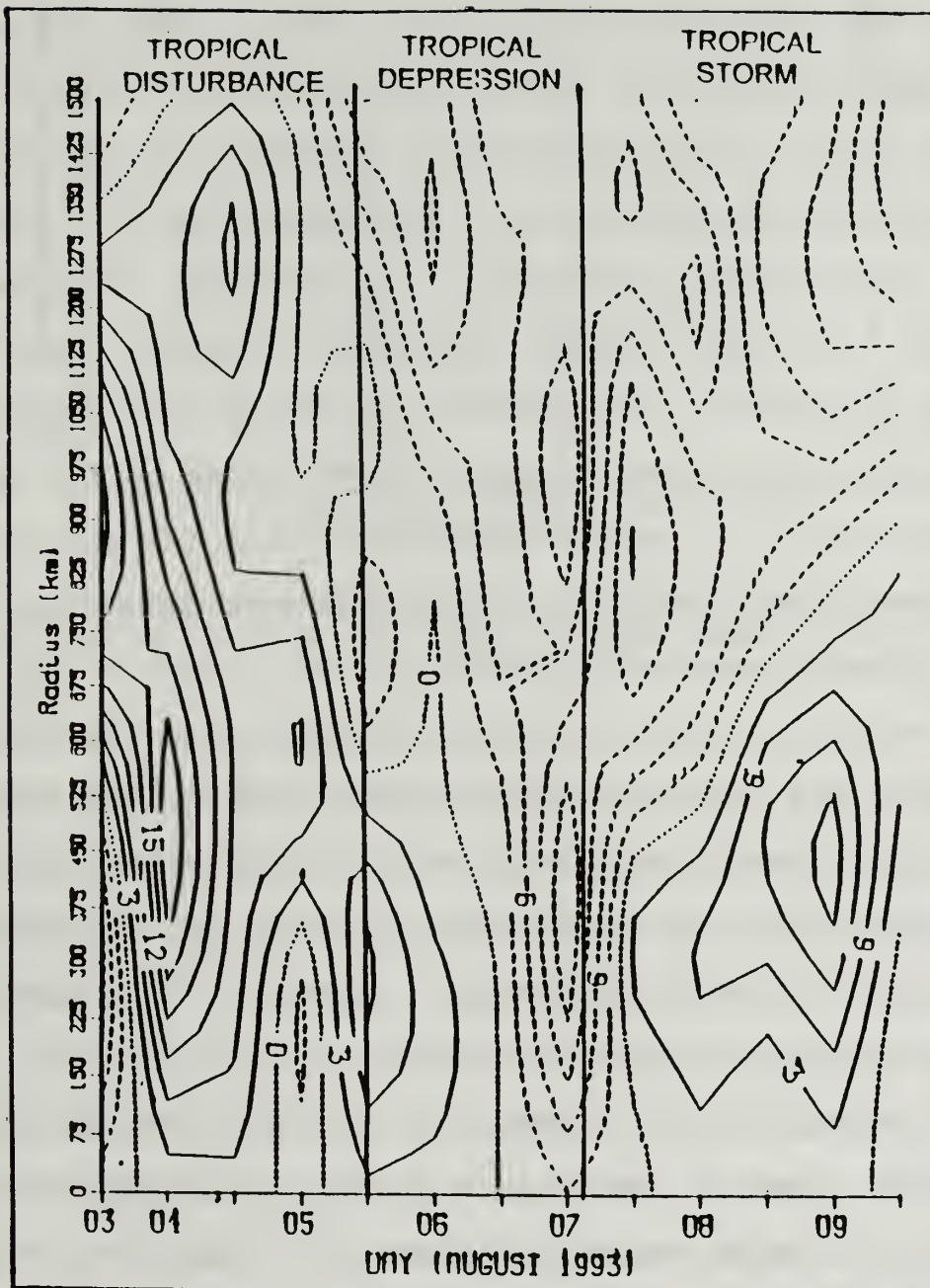


Figure 7. 200 mb Eddy Flux Convergence (EFC) (contour interval $3 \text{ m s}^{-1} \text{ d}^{-1}$) from 12 UTC 3 August to 12 UTC 9 August 1993 for TC Steve calculated from the multi-quadric analyses. Solid (dashed) lines represent increasing (decreasing) cyclonic tendencies.

greater than $0.3 \times 10^{-5} \text{ s}^{-1}$. Convergence and relative vorticity values over pre-Steve for this stage (Fig. 8) barely meet the requirements of Zehr (1992). He did not find threshold values for upper-level relative vorticity because there was little difference in patterns for developing and non-developing disturbances. Although there was a weak signal for upper-level divergence, the standard deviations were large. At upper levels, divergence occurred over the pre-Steve disturbance (not shown) but the relative vorticity was cyclonic from 00 UTC 4 August to the end of this stage. This could be due to a strong northerly wind on the western side of the pre-Steve disturbance, which is also where the vertical wind shear is the strongest.

Analysis of Geostationary Meteorological Satellite (GMS) visible and infrared (IR) imagery showed that a mid-level mesoscale convective vortex (MCV) was associated with the pre-Steve MCS (Fig. 9). MCVs may form in the stratiform region of MCSs and are inertially stable, warm-core vortices that have their strongest cyclonic circulation at mid levels (450-700 mb), but may extend downward to near the surface (Menard and Fritsch 1989). MCVs are normally detected in daytime satellite imagery when the convective minimum occurs and the overlying cirrus canopy either dissipates or is sheared away. MCVs do not form in every MCS and their detection is complicated by the lack of observational data and the cirrus canopy that normally covers the MCV. It is possible that the

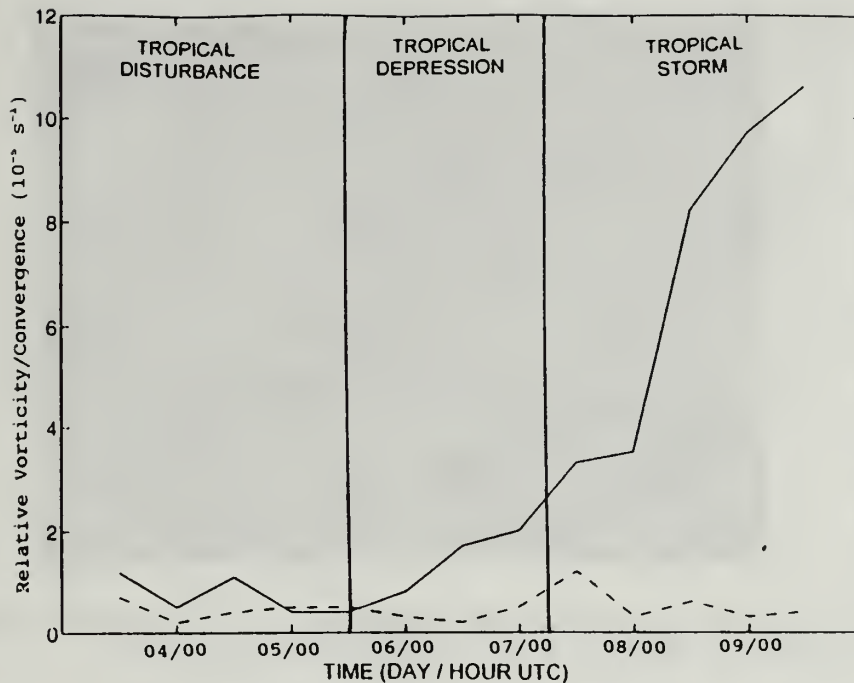


Figure 8. Relative vorticity (solid, 10^{-5} s^{-1}) and convergence (dashed, 10^{-5} s^{-1}) at 850 mb over TC Steve from 12 UTC 3 August to 12 UTC 9 August 1993 calculated from the multi-quadric analyses.

pre-Steve MCV extended downward to the surface, but this could not be confirmed due to the lack of observations.

The MCVs can last for several days and can initiate development of subsequent convection (Bartels and Maddox 1991). The initiation of the MCV requires large values of convergence and upward vertical motion and is accompanied by the increase of local relative vorticity maximum, which is a positive influence on tropical cyclone development (Zehr 1992). The southwest monsoon surge in Fig. 4a may have provided the necessary convergence for the MCV to form in pre-Steve.

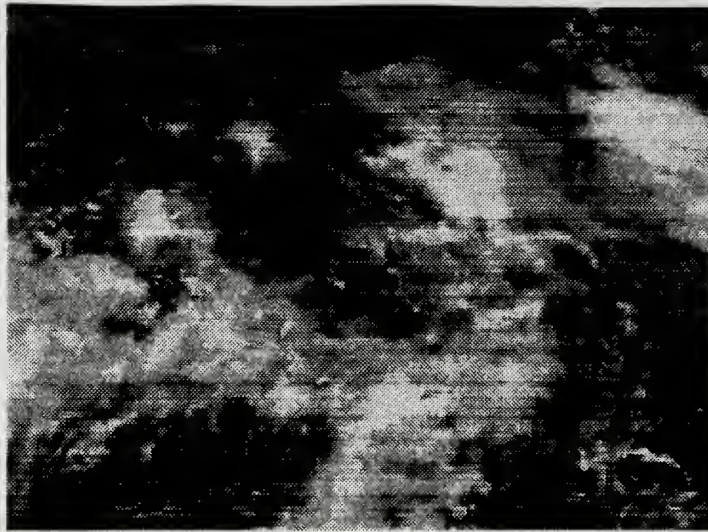


Figure 9. Visible satellite imagery at 0130 UTC 4 August 1993 showing the pre-Steve MCV (marked with 'x').

A cirrus cloud shield reformed above the vortex each night with the areal coverage of cold cloud-top temperatures increasing from the previous night (see Fig. 10). The minimum cloud-top temperatures for pre-Steve (Fig. 11) were slightly warmer than for Typhoon Robyn (Fig. 11), which indicates the deepest convection of Robyn was only slightly deeper than the deepest convection of pre-Steve. This difference in cloud-top temperatures was mainly due to daytime warming of cloud tops for pre-Steve, so the convection was not as deep during the day. By contrast, a significant diurnal cloud-top temperature trend was not observed for Typhoon Robyn.

A large number of convective clusters occurred in the inflow that was east to southeast of Typhoon Robyn. Why one cluster develops over another cluster is an unanswered question. A possible answer is Rossby wave dispersion of

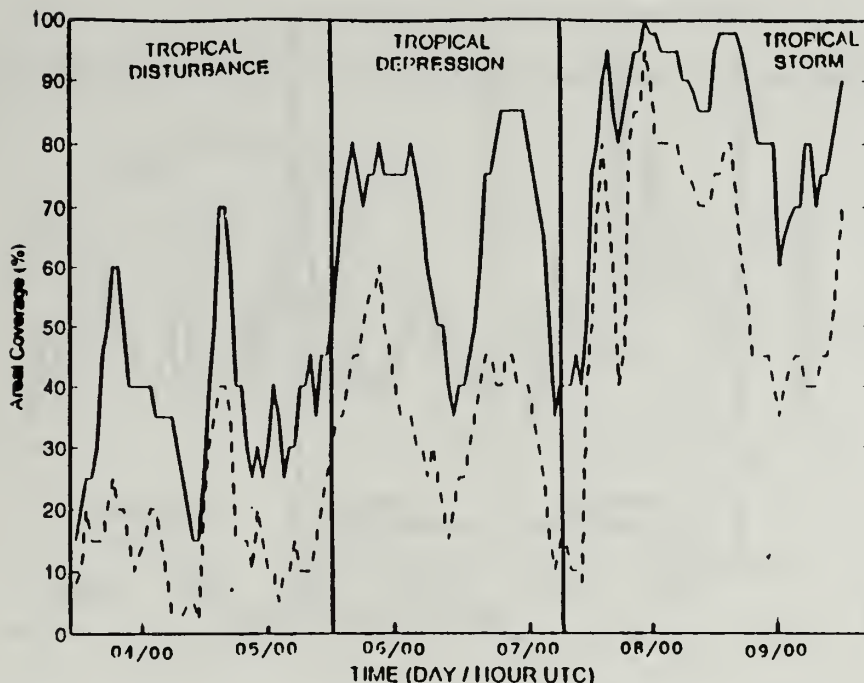


Figure 10. Percentage of cloud tops in a 4 deg. lat. box centered on TC Steve with IR satellite imagery temperatures less than -65°C (solid) and less than -85°C (dashed) for 12 UTC 3 August to 12 UTC 9 August 1993.

energy. The large outer circulation of Typhoon Robyn is similar to that of a monsoon gyre. Lander (1993) defined a monsoon gyre as a large-scale, solitary, cyclonic gyre originating *in situ* that is isolated over water (i.e., a north-south ridge of high pressure disconnects it from the low-pressure area over Asia). The dispersion of energy from the monsoon gyre is manifest as a Rossby wave train that consists of a peripheral anticyclone and a second cyclone farther to the southeast, which agrees well with typical patterns (Carr and Elsberry 1994). The outer circulation of a TC with a large spatial scale, such as Typhoon Robyn, might also generate a Rossby wave train similar to that of the

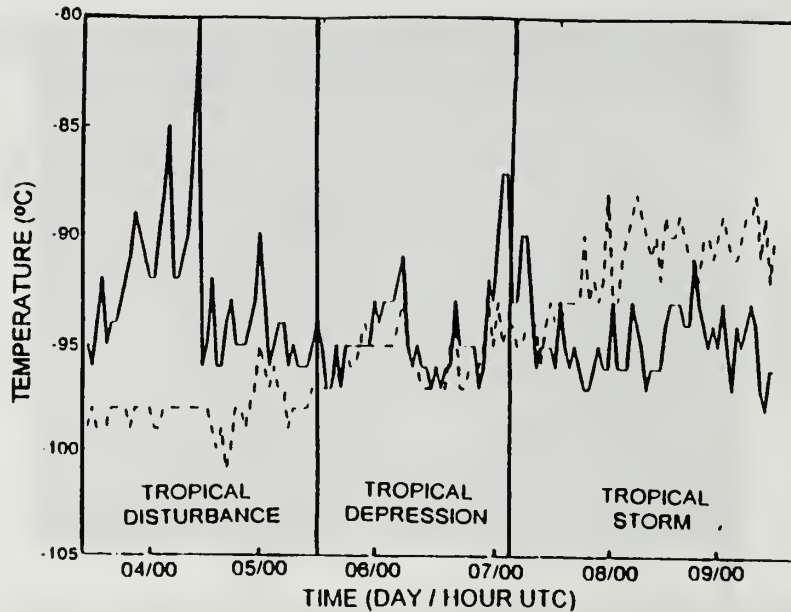


Figure 11. Minimum cloud top temperatures ($^{\circ}\text{C}$) for TC Steve (solid) and TC Robyn (dashed). Temperatures were obtained from IR satellite imagery each hour.

monsoon gyre. A TC embedded within the monsoon gyre, or the inner core of TC with a large monsoon gyre-like outer circulation, might result in the generation of two Rossby wave trains with different wavelengths. If the trough of the shorter wavelength TC wave train overlaps the ridge of the longer wavelength outer circulation (Fig. 12a), TC formation may be suppressed due the ridge inhibiting the positive effects of the trough (i.e., increased low-level convergence). It is also possible that the TC Rossby wave train trough does not overlap with the larger wave train at all (Fig. 12b). This could result in a localized area of increased low-level convergence and relative vorticity leading to deep convection

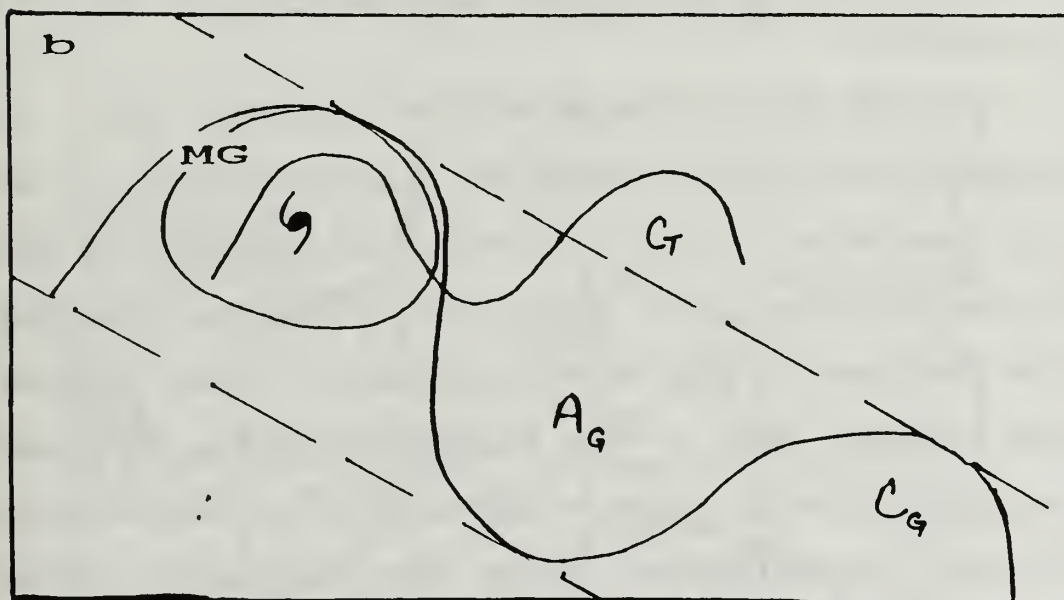
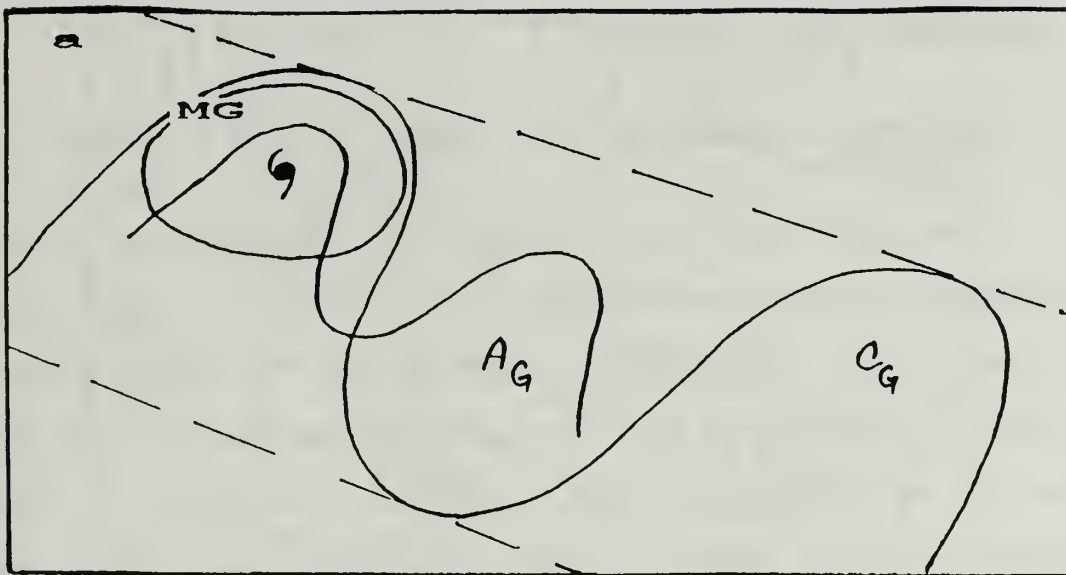


Figure 12. Schematic of Rossby wave train dispersion: (a) trough (C_T) of wave train generated by TC overlaps with anticyclone (A_G) of wave train generated by monsoon gyre; and (b) trough of wave train generated by TC does not overlap with wave train generated by monsoon gyre.

and the formation of a TC, even in moderate to strong vertical wind shear environments.

B. TROPICAL DEPRESSION (TD) STAGE (12 UTC 5 AUGUST - 00 UTC 7 AUGUST)

The pre-Steve disturbance was upgraded to a TD with maximum sustained winds of 20 kt at 12 UTC 5 August (Fig. 3). From 12 UTC 6 August to the end of the TS stage, Steve moved west-northwest at 9 kt. Because Typhoon Robyn moved northwest at 12 kt throughout the stage, the influence of Robyn on Steve's track was diminishing as the separation distance increased from 14.8 deg. lat. to 15.8 deg. lat. at the end of the period.

The 00 UTC 7 August 850 mb analysis (Fig. 13a) is representative of the persistent, low-level synoptic condition for this period. Steve was still east-southeast of Robyn and in the weak portion of the monsoon trough and tracking under the influence of the east-southeasterly winds located along the southern edge of the subtropical ridge. Although the subtropical ridge position and overall low-level circulation of the pre-disturbance stage were maintained during this depression stage, Robyn was weakening the western portion of the ridge, which caused the ridge to shift north. A near-equatorial anticyclone that had developed south of the disturbance shifted westward until it provided the southerly inflow to Steve on 12 UTC 5 August (not shown). An extensive

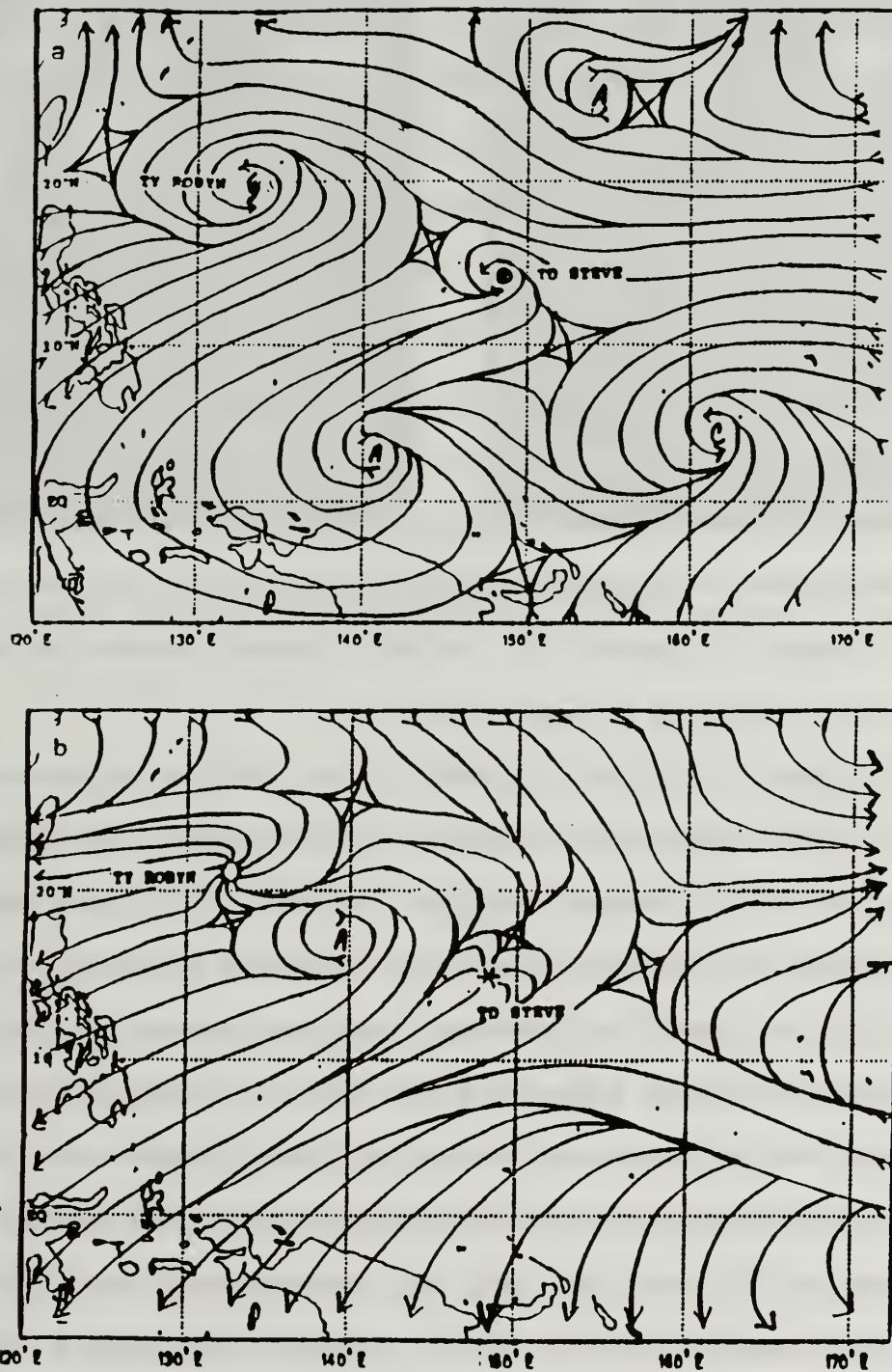


Figure 13. Streamline analyses over the western North Pacific for 00 UTC 7 August 1993 at (a) 850 mb, and (b) 200 mb.

layer of low clouds that was evident in the IR imagery was associated with this anticyclone (Fig. 14a). Visible imagery revealed multilayered cloudiness with multiple breaks (Fig. 14b). The synoptic observations from island stations located from southeast of Steve to south-southwest of Robyn identified the clouds as cumulus (with small vertical extent), stratocumulus, altocumulus, altostratus, cirrus and cirrostratus. The soundings from Chuuk, which was southeast of TD Steve, and Guam, which was located to the east, have a new area of drier air (dewpoint depression between 5-10°C) between 850 to 700 mb during this stage (not shown). However, the multiple layers of clouds indicate that moisture was available through a deep layer.

During 12 UTC 5 August to 00 UTC 7 August when the anticyclone appeared to govern the inflow to pre-Steve, small bands of convection located between pre-Steve and Robyn dissipated during the day and did not redevelop at night. Although the small cloud band dissipation was probably due to subsidence between Robyn and pre-Steve, no apparent effect was evident on larger bands of convection, on Robyn, or on Steve. The air diverging out of the near-equatorial anticyclone may have been more stable than the surrounding tropical air, so that the vertical wind shear generated by Robyn was strong enough to prevent new areas of convection from redeveloping between Robyn and Steve at night. Strong vertical wind shear

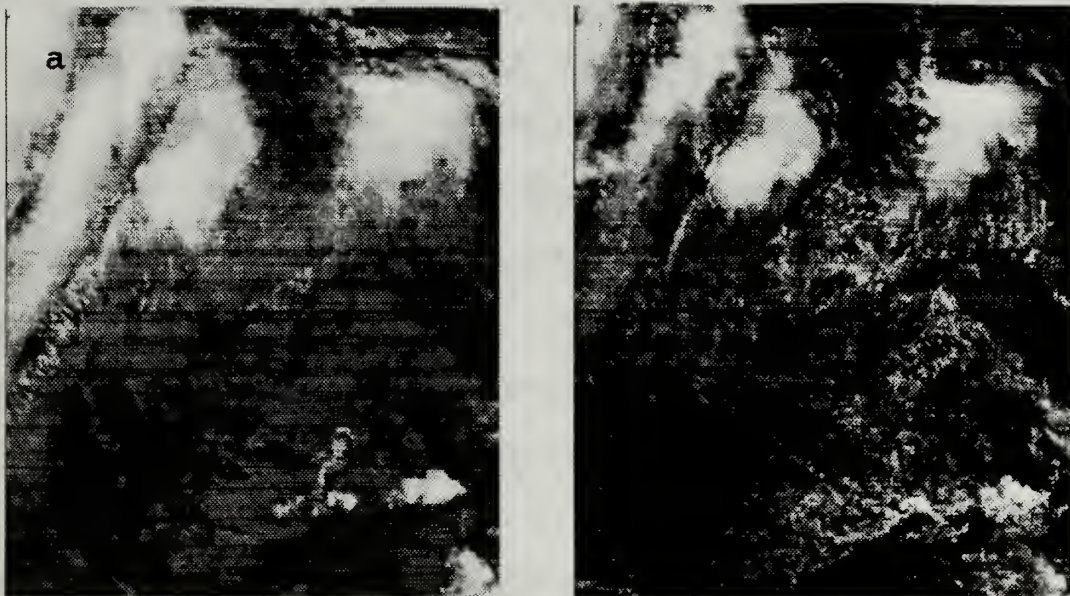


Figure 14. (a) IR and (b) visible satellite imagery for 0030 UTC 6 August 1993 showing low-level cloudiness associated with 850 mb equatorial anticyclone. TD Steve is located in the upper right hand corner.

can be detrimental to updraft growth in weakly buoyant environments, inhibiting the convective plume (NWS 1993).

The nighttime maxima in areal extent of cold cloud-top temperatures for Steve (Fig. 10) continued to increase, and the corresponding nighttime minimum in cloud-top temperature (Fig. 11) continued to get colder. The diurnal range between the daytime (nighttime) increase (decrease) in minimum cloud-top temperatures generally decreased during this period. The minimum cloud top temperatures for Steve and Robyn became more similar during this period. That is, the deepest convection in TD Steve was nearly as deep as that of Typhoon Robyn (Fig. 11). The cloud layers to the southwest of Steve started to dissipate after 12 UTC 6 August and the area was nearly clear

by 0230 UTC 7 August. Once the anticyclone was located south-southeast of Steve, small areas of convection started to develop in the area separating the two storms.

A second surge, this time from the east-southeast, led to an increase of east-southeasterly 850 mb winds from 15 kt to 25 kt to the east of Steve. The surge occurred at about 12 UTC 6 August to 00 UTC 7 August and may have been responsible for the increase in convection that recovered the low-level circulation center (LLCC).

TUTT-associated divergence support continued until 12 UTC 6 August (not shown) when the TUTT axis shifted eastward from Steve. A nearly uniform north to northeasterly flow was over Steve through the remainder of this stage, as in the 00 UTC 7 August 200 mb analysis in Fig. 13b. This flow was primarily produced by the outflow from Robyn, and this influence was clearly identifiable in the looped satellite images during this period. An upper-level anticyclone did not develop over Steve during this period. Instead, the most appropriate representation of available observations was an upper-level point divergence. Upstream flow against the impinging northeasterly flow is represented by a bow-shaped interaction zone. The strongest outflow from pre-Steve was toward the southwest. Thus, the vertical wind shear from Robyn, in combination with the TUTT, probably had more of an inhibiting effect on the further development of TD Steve than during the disturbance stage.

The vertical wind shear over TD Steve and over Guam (Fig. 5) increased during this stage. After 12 UTC 6 August, Zehr's (1992) threshold value of 12.5 m s^{-1} was significantly exceeded. The increase in magnitude of the vertical wind shear did not stop the maximum low-level wind velocity (intensity) of TD Steve from increasing (Fig. 6) during this stage.

Although the EFC near the center was first positive, it became negative by the end of the stage (Fig. 7). The negative EFC near the center occurred during the daytime convective minimum. Also farther from the center, the EFC became negative. Zehr's development requirements for 850 mb relative vorticity and convergence, which were listed in the disturbance stage, were met during this stage (Fig. 8). Cyclonic relative vorticity was again present at 200 mb along with divergence (not shown). For the majority of the TD stage of pre-Steve, the low-level circulation center (LLCC) was partially exposed. This differs from the disturbance stage during which there was a diurnal trend to the exposure of the MCV, primarily due to the daytime convective minimum. The diurnal convective trend was the primary determinant of how much of the LLCC was exposed, i.e., the LLCC was least exposed during nighttime hours.

The upper-level outflow for Typhoon Robyn increased on the eastern side and produced strong vertical wind shear that extended a considerable distance to the east and southeast of

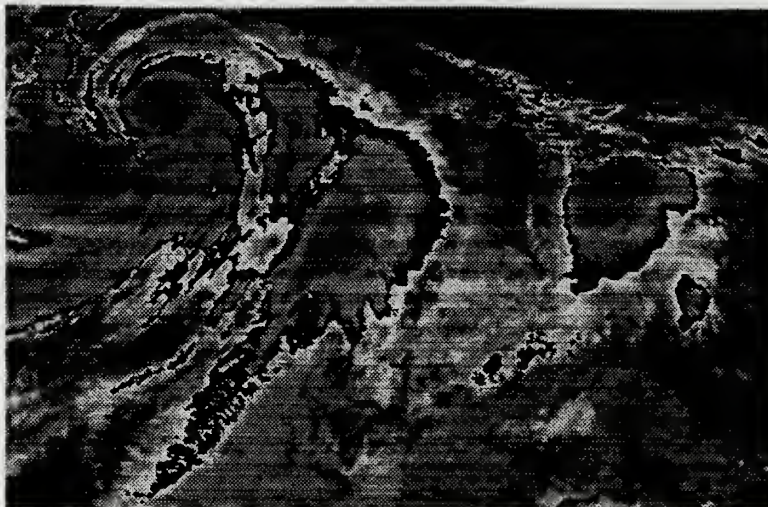


Figure 15. Enhanced IR satellite imagery for 1830 UTC 5 August 1993. Typhoon Robyn is located in upper left corner and TD Steve is located on right side. Cloud temperatures less than -65°C were enhanced. Notice the location of deep convection in relation to the partially exposed low-level circulation of TD Steve.

Robyn. This vertical wind shear combined with the shear generated by the TUTT caused the LLCC to be partially exposed for most of the period from 2130 UTC 5 August to 0930 UTC 7 August. From 1030-1930 UTC (nighttime) 5 August, the convection rebuilt over the center of the LLCC (Fig. 15) with only the western to northern edges of the LLCC exposed. The LLCC was fully exposed between 0030-0630 UTC 6 August (Fig. 16).

While the LLCC was partially exposed, the deepest convection was located either over the vortex center or over the southern portion of the vortex. This could allow the latent heat released within the convection to be circulated around the vortex, which may ensure that the vertical coupling



Figure 16. Visible satellite imagery for 0030 UTC 6 August 1993 showing the exposed LLCC of TD Steve.

of the system is never completely broken. A schematic of this partially exposed low-level circulation with upper-level subsidence on one side is shown in Fig. 17a.

The location of the deepest convection over the partially exposed vortex, or east and south of the exposed circulation center, appears to be important to maintaining Steve. If the upper-level outflow from Steve clashes with the outflow from Robyn, it would force the flow downward. If the flow is forced downward over the exposed LLCC (Fig. 17a), it would meet ascent over the low-level circulation, and may provide a mid-level outflow of warm air to the outer edges of the circulation to then be circulated around the edges of TD

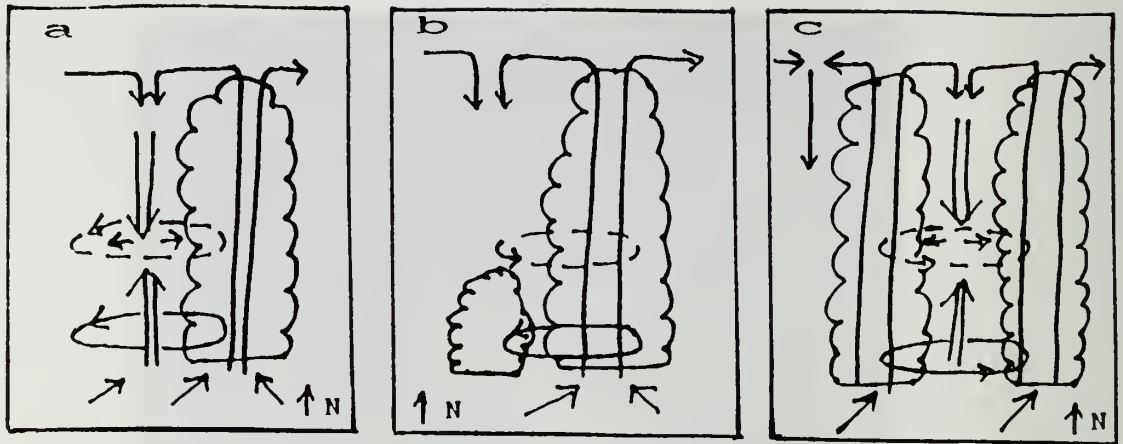


Figure 17. Schematic of impinging upper-level flow causing (a) subsidence within the center of the LLCC and convection restricted to one side of the LLCC; (b) subsidence on the edge of the LLCC with convection near the center and along one side of the LLCC; and (c) fully covered LLCC with TC outflow forcing descent outside of the system.

Steve. Since the descending air warms, it would help build or maintain a warm mid-level core which would lead to decreasing surface pressure. If the flow is forced downward over the northern or western edge of the vortex (Fig. 17b), the warm air would again be available for circulation around the mid-level circulation, and would aid the convection near the center in maintaining the warm core and would prevent the flow from Robyn from further exposing the LLCC. The low-level monsoon trough is necessary to provide low-level convergence, and the southwest monsoon flow into the storm provides the moisture necessary for the deep convection. For the two scenarios discussed above, the warm air descending into the warm core combining with the latent heat released from the convection must be strong enough to decrease the surface

pressure to account for the increase in intensity that was observed for TD Steve under the strong vertical wind shear conditions. If the LLCC is covered (Fig. 17c), the forced descent outside of the convection would decrease the effectiveness of the vertical shear from decoupling the system. A covered LLCC would protect the circulation against the shear better than having the convection along the edge (Fig. 17a). Having the convection rebuild over the center would also be more effective in maintaining a minimum of vertical tilt over the system.

C. TROPICAL STORM (TS) STAGE (03 UTC 7 AUGUST - 12 UTC 9 AUGUST)

TD Steve was upgraded to TS at 03 UTC 7 August. Steve was now southeast of Robyn (Fig. 3) and the separation distance between the two storms was increasing. The combination of Typhoon Robyn, a midlatitude cyclone that developed north of Robyn during this period, and TS Steve resulted in a complete break in the subtropical ridge. As the subtropical ridge axis became oriented northwest to southeast, Steve continued to move west-northwest at 9 kt during this stage. Typhoon Robyn moved northwest and then recurved from 18 UTC 8 August to 12 UTC 10 August. The separation distance between Robyn and Steve increased from 15.8 to 17.3 deg. lat. by the end of this stage. Thus, the inhibiting effects of the vertical wind shear on Steve were reduced early in TS stage so that

conditions became optimal for normal or even rapid development.

As the storms separated, Steve was actually in the flow around the southern portion of the 850 mb subtropical ridge and was not significantly influenced by the circulation of Robyn (Fig. 18a). The low-level equatorial anticyclone was located more south-southeast of Steve, which increased the proportion of the inflow that was associated with the cross-equatorial flow and reduced the portion out of the anticyclone. This allowed more unstable air to flow into Steve and enhanced the outer circulation. At upper levels (Fig. 18b), the TUTT axis shifted farther to the east of Steve. The northeasterly flow west of the TUTT combined with the flow around the upper-level anticyclones, and this took the form of a bow wave as it goes around Steve (Fig. 19).

Strong vertical shear over Steve was being generated by Robyn and the TUTT during the beginning of this period. A partially exposed LLCC was identified in visible satellite imagery until 0930 UTC 7 August (not shown). Cirrus streaks from the upper-level circulation of Robyn extended to within 3-5 deg. lat. of Steve through most of the period. Robyn's effect on Steve weakened through the period as the distance between the storms increased. An anticyclone was analyzed over Steve at 12 UTC 7 August (not shown), and that interpretation was confirmed in the satellite imagery. The outflow at 0630 UTC 8 August was restricted from west to north

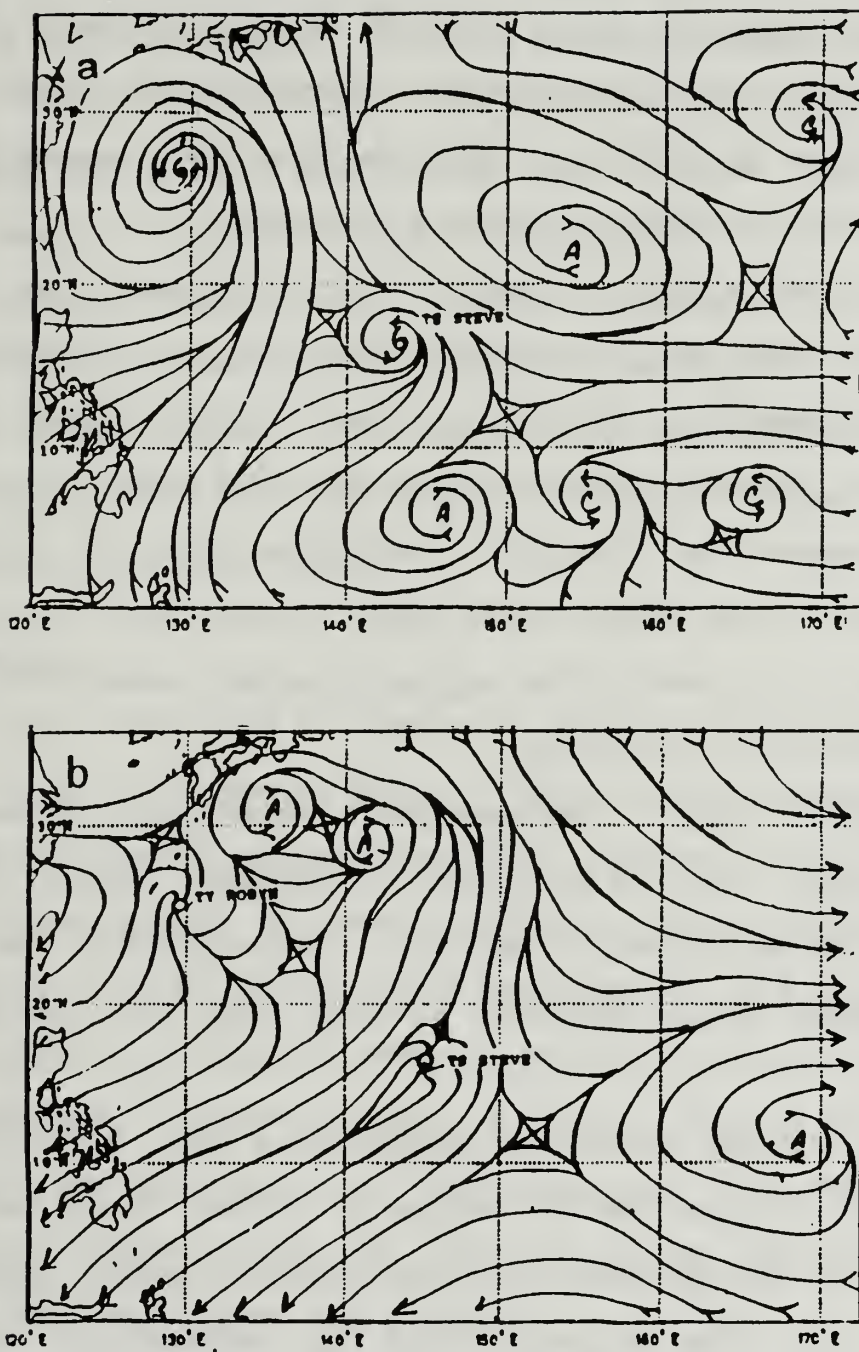


Figure 18. Streamline analyses over the western North Pacific for 12 UTC 8 August 1993 at (a) 850 mb, and (b) 200 mb.

of the center due to the vertical shear from Robyn and the TUTT. Thus, the outflow from Steve was limited to the southern quadrant until 12 UTC 8 August, when it became broader, but still constrained toward the southwest. By the end of the period, the outflow area had expanded in the western and northern quadrants of Steve.

As seen in Fig. 5, the vertical wind shear over TS Steve and Guam was still strong. Due to an earthquake, Guam soundings were not available after 00 UTC 8 August. TS Steve was also passing close to Guam at this time. The vertical shear caused by synoptic conditions did not decrease as expected. The upper-level anticyclone over TS Steve was successful in pushing the impinging upper-level flow away from the center of the vortex.

The EFC (Fig. 7) becomes positive near the center through this stage, which is conducive to intensification. At larger radii, the EFC is still negative. The effects of the vertical wind shear still dominate farther from the center of the system.

The minimum cloud-top temperatures (Fig. 11) continued to decrease during the TS stage of Steve, with values very similar to the minimum cloud-top temperatures of Typhoon Robyn (Fig. 11). The minimum cloud-top temperature for Typhoon Robyn was undergoing a warming trend as Robyn moved over relatively cooler water. These minimum cloud-top temperatures for Steve were generally west to north of the vortex center

(not shown). The outflow toward the northeast of Steve was restricted to the area of the bow wave (Fig. 18b).

From 11 to 12 August, TC Steve moved northward out of the monsoon trough circulation. The moderate to strong vertical wind shear due to the upper-level anticyclones over Asia and to the north of Steve was able to expose the LLCC. The deep convection was located over the southern edge of the LLCC, as in Fig. 17b, and then the system became decoupled and TC Steve dissipated over water. This highlights the importance of the monsoonal circulation with moist low-level inflow for storm maintenance/intensification.

D. SUMMARY

TC Steve developed southwest of Guam in the monsoon trough in the wake of Typhoon Robyn. Upper-level divergence and enhanced low-level convergence were positive effects on the initial development of Steve. However, strong vertical wind shear generated by large-scale environment (i.e., the TUTT, Robyn, large-scale anticyclonic flow aloft) inhibited, but did not terminate, the development of Steve. Due to this shear, the LLCC was partially to fully exposed for most of the depression stage, and the development of an upper-level anticyclone over Steve was delayed.

Several possible mechanisms appeared to maintain the circulation of Steve against the inhibiting effects of the shear. The maintenance of deep convection over the center or

just south of the LLCC may have assisted in keeping the system vertically coupled and prevented the destruction of the warm core. The diurnal maximum of convection, which was documented by the high spatial and temporal resolution satellite imagery, assisted in fighting off the shear when the convection redeveloped over the vortex center during nighttime hours. This would strengthen the vertical coupling by producing/intensifying a warm core at mid-levels. The interaction between the impinging flow aloft and the convection during the tropical depression stage may have forced downward motion that produced warming over the LLCC (Fig. 17a). This warming combined with latent heat released due to convection had to be strong enough to maintain a warm core and assist in increasing the intensity of the TD. Although downdrafts may have been introduced within the convection due to the drier mid-level air for entrainment, the vertical shear did not ventilate Steve or fully decouple the system. Presumably this was due to the low-level circulation and moisture supply from the monsoon trough environment that sustained Steve against the inhibiting effects aloft. The location of a TC within a very active monsoon trough environment appears to be a key factor for determining the ability of a developing system to overcome inhibiting vertical shear.

The location of the developing TC may depend on Rossby wave dispersion. The outer circulation of TC with a large spatial scale, such as Typhoon Robyn, might generate a Rossby

wave train similar to that of the monsoon gyre. If the trough of the Rossby wave train generated by the inner core does not overlap the ridge of the longer wavelength outer circulation Rossby wave train (Fig. 12b), a localized area of increased low-level convergence and relative vorticity could lead to deep convection and the formation of a TC, even in moderate to strong vertical wind shear environments. This appears to have occurred for TC Steve, which formed north-northeast of the low-level equatorial anticyclone associated with the monsoon gyre.

Two other TC cases in which strong vertical wind shear effects were present will be examined to determine if similar physical processes occurred.

VI. TROPICAL CYCLONE ZOLA

A. TROPICAL DISTURBANCE STAGE (06 UTC 15 AUGUST TO 00 UTC 17 AUGUST)

The pre-Zola disturbance was first detected as a persistent cloud cluster to the southeast of TS Yancy in a region of monsoonal convective activity. On 15 August 1990, TS Yancy was located at the center of a large monsoon gyre (Fig. 19a), and the LLCC associated with the pre-Zola disturbance was to the north of the strong monsoonal convection. At 12 UTC 16 August, TS Yancy was upgraded to a typhoon.

After briefly tracking eastward from 06 UTC 15 August to 18 UTC 15 August, the pre-Zola cloud cluster started moving north-northeastward just west of the Northern Marianas Islands in the low-level inflow to Typhoon Yancy (Fig. 20). The cyclonic turning in the track was evidently due to the pre-Zola disturbance being within the low-level circulation of Yancy as the separation distance between the two systems was only 7 deg. lat. at 06 UTC 15 August. A true binary interaction between Typhoon Yancy and pre-Zola did not occur due to the large difference in the system intensities. The pre-Zola disturbance developed closer to the leading TC than the pre-Steve disturbance did, which developed at a distance of 11.9 deg. lat. The low-level circulation of Typhoon Yancy

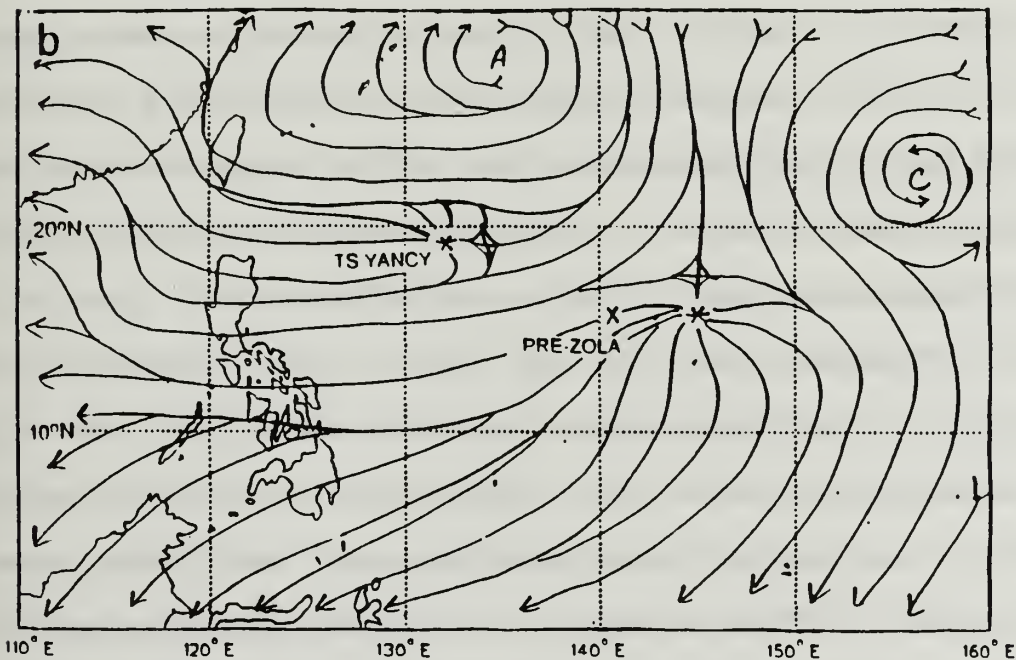
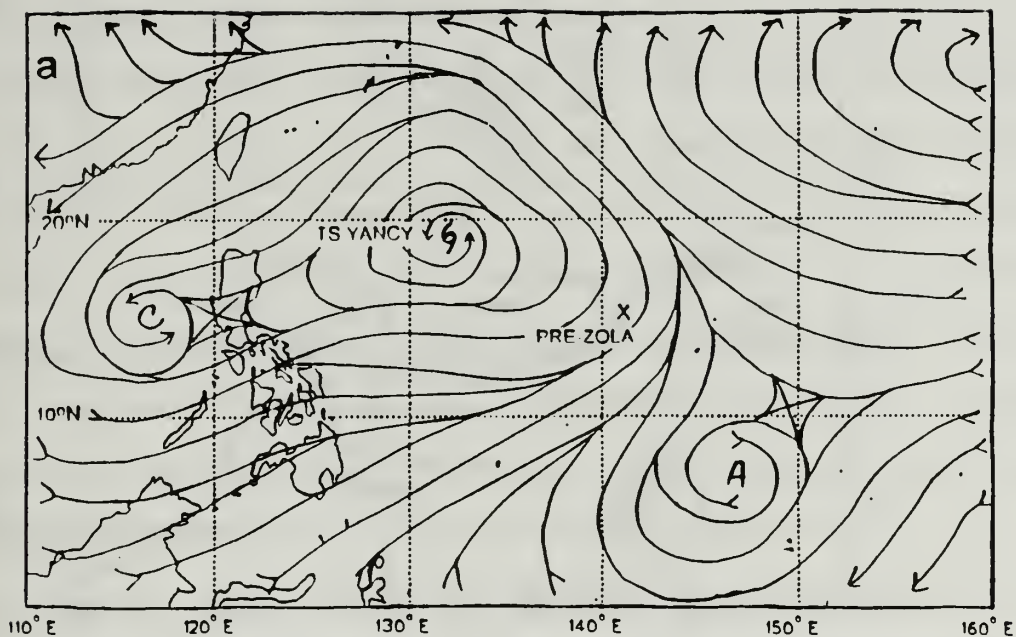


Figure 19. Streamline analyses over the western North Pacific for 12 UTC 15 August 1990 at (a) 850 mb, and (b) 200 mb.

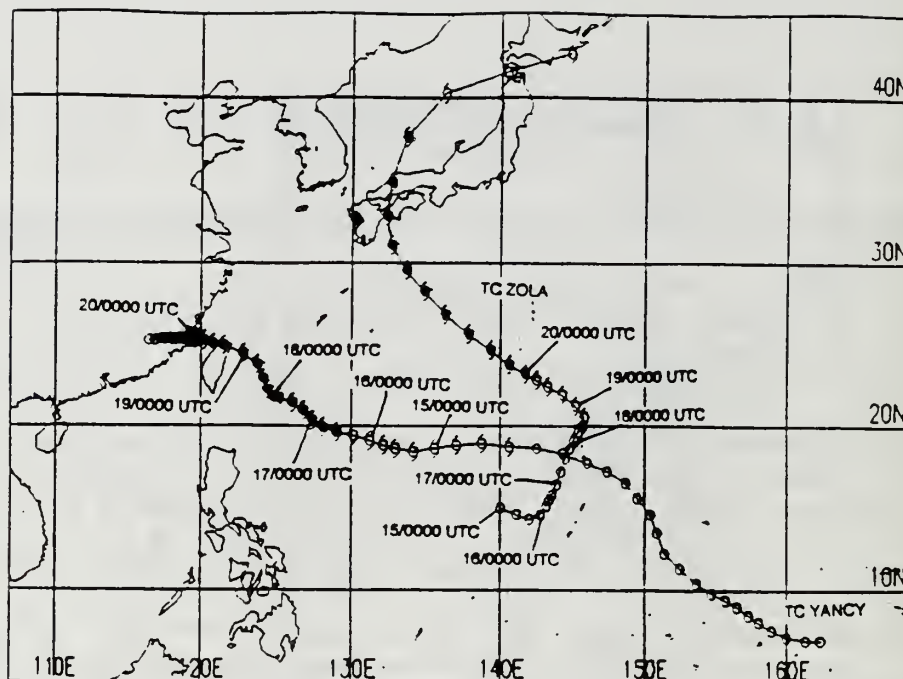


Figure 20. JTWC best tracks for TC Yancy and TC Zola during August 1990 with symbols as in Fig. 3.

appeared to control the initiation and maintenance of pre-Zola to 00 UTC 16 August, while the initiation and maintenance of the pre-Steve disturbance was a function of Typhoon Robyn and the monsoon trough. This separation distance does not meet the minimum separation distance (9 deg. lat.) that is required for TC development in the wake of the leading TC (Briegel 1993). The requirement was met later as the separation distance increased to 15 deg. lat. at 00 UTC 17 August when Zola was moving north-northeastward and Yancy was moving westward. This movement of Typhoon Yancy lasted for three days under the influence of the subtropical ridge (Fig. 19b).

Pre-Zola formed over a warm sea. During the disturbance stage, the sea-surface temperature (SST) ranged from 29.5°C to

30.5°C, which well exceeds the minimum SST of 26.5°C (Frank 1987).

TCM-90 analyses were compared to hand-drawn analyses at both 850 mb and 200 mb. There was good agreement on the location of the circulation centers and in the overall patterns. Thus, the TCM-90 analyses were used to create the analyses for this case. The pre-Zola disturbance did not appear in early analyses until 00 UTC 16 August, perhaps because the pre-Zola disturbance was small and not resolved by the observations.

At 850 mb (Fig. 19a), the monsoon gyre extended from a cyclone in the South China Sea east-northeastward to Typhoon Yancy and then east-southeastward to the region of pre-Zola. An equatorial anticyclone was located to the southeast of Typhoon Yancy with strong cross-equatorial southwesterly flow into the monsoon gyre. This pattern is similar to the Rossby wave train dispersion pattern of Fig. 12b except that pre-Zola was located between Typhoon Yancy and the equatorial anticyclone. TD Zola is on the eastern periphery of the monsoon gyre. The monsoon trough slowly expanded to the east-southeast throughout the period. The subtropical ridge was northeast of Typhoon Yancy and ridging extended north of Yancy into China. The ridging north of Yancy weakened through the period as a midlatitude trough moved into the Yellow Sea. This synoptic situation was similar to that of the pre-Steve disturbance.

At 200 mb (Fig. 19b), a large TUTT cell was northeast of the pre-Zola low-level disturbance and an anticyclone that was part of the subtropical ridge was to the northwest of pre-Zola. A divergent point outflow above pre-Zola is generally consistent with the divergent flow between the TUTT cell and the anticyclone to the north. A weak northerly flow to the north was deflected around the divergent point outflow area. The TUTT cell slowly moved west-northwestward. The contribution of the TUTT to the development of pre-Zola appears to be similar to the TUTT influence associated with the pre-Steve disturbance. Outflow from Typhoon Yancy was strongest on the west side at the beginning of the period but increased outflow toward the south developed during the period. This outflow from Yancy did not contribute to the vertical wind shear over the pre-Zola disturbance, which appeared to be due to the TUTT and the upper-level anticyclone associated with the monsoon gyre. This is again similar to the pre-Steve disturbance in which the TUTT produced the vertical shear over pre-Steve vice Typhoon Robyn.

The Zehr (1992) general requirements for 850 mb relative vorticity and 850 mb convergence were given in Chapter IV. As seen in Fig. 21, the values found for pre-Zola generally exceeded Zehr's requirements by a significant amount. These values have typically been calculated on a grid with 2.5 deg. resolution, while the resolution of the TCM-90 analyses for this case study is 50 km. The values are interpolated to the

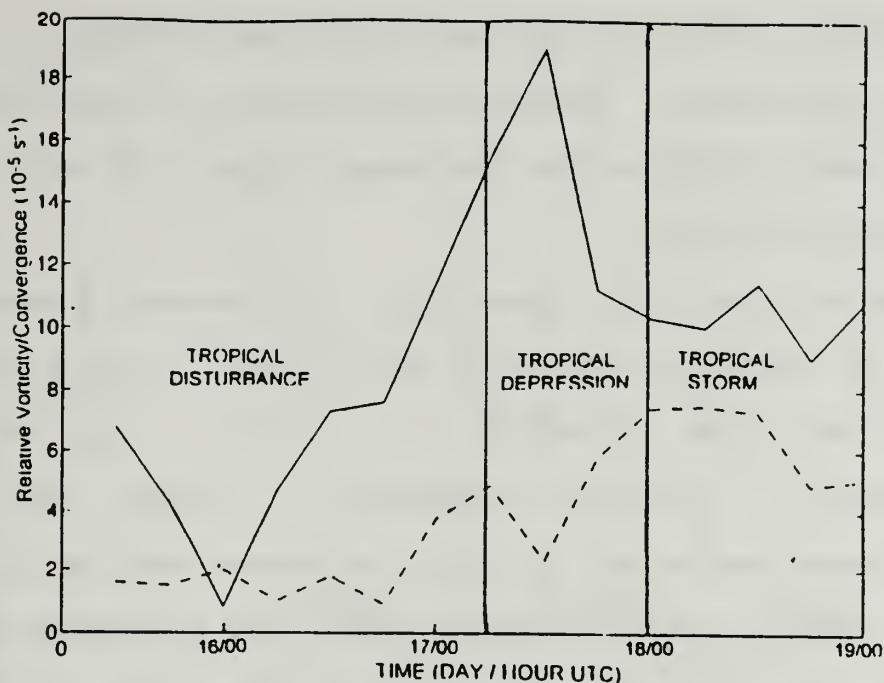


Figure 21. Relative vorticity (solid, 10^{-5} s^{-1}) and convergence (dashed, 10^{-5} s^{-1}) at 850 mb over TC Zola from 12 UTC 15 August to 00 UTC 19 August 1990 calculated from the TCM-90 analyses.

pre-Zola location within one half degree, and temporal resolution is 6 h. Since the values for pre-Zola were calculated over smaller distances, the magnitude will be generally larger than the Zehr values.

At 200 mb (not shown), anticyclonic relative vorticity and divergence were found over the pre-Zola area. However, the relative vorticity was cyclonic from 12 UTC to 18 UTC 16 August, which appears to be due to the horizontal shear in the area (i.e., stronger winds located on the western side).

The upper-air soundings from the islands to the southeast (Guam at 13.6°N , 144.8°E and Chuuk at 7.5°N , 152°E) and southwest (Yap at 9.5°N , 138.1°E and Palau at 7.3°N , 134.5°E)

of pre-Zola indicate that moisture was available to the mid levels (not shown). Dewpoint depression $< 5^{\circ}\text{C}$ extended upward to at least 300 mb to the southwest of pre-Zola and to 400-500 mb to the southeast.

The vertical wind shear (Fig. 22) generally exceeded the 12.5 m s^{-1} threshold value of Zehr (1992). It did decrease to less than this threshold 6 h prior to pre-Zola being designated a tropical depression. Thus, the pre-Zola disturbance was under strong to moderate vertical wind shear during most of the disturbance stage. As indicated above, the shear was produced by the upper-level flow between the anticyclone and the TUTT. The outflow from Typhoon Yancy was constrained on the eastward side (Fig. 19b). This appears to be the reason pre-Zola could develop within 10 deg. lat. of Typhoon Yancy. This is very similar to the moderate to strong vertical wind shear that influenced the development of the pre-Steve disturbance. Key observations were obtained by a ship that was moving northward along 136°E from 16.9°N to 21°N , which put it between pre-Zola and Typhoon Yancy. Although the trends are similar, the vertical wind shear recorded by the ship (Fig. 22) was generally less than over pre-Zola. This was due to the ship being located closer to Typhoon Yancy and away from the upper-level flow producing the shear over pre-Zola.

The maximum low-level wind velocity (intensity) of pre-Zola remained steady through 12 UTC 17 August even though the

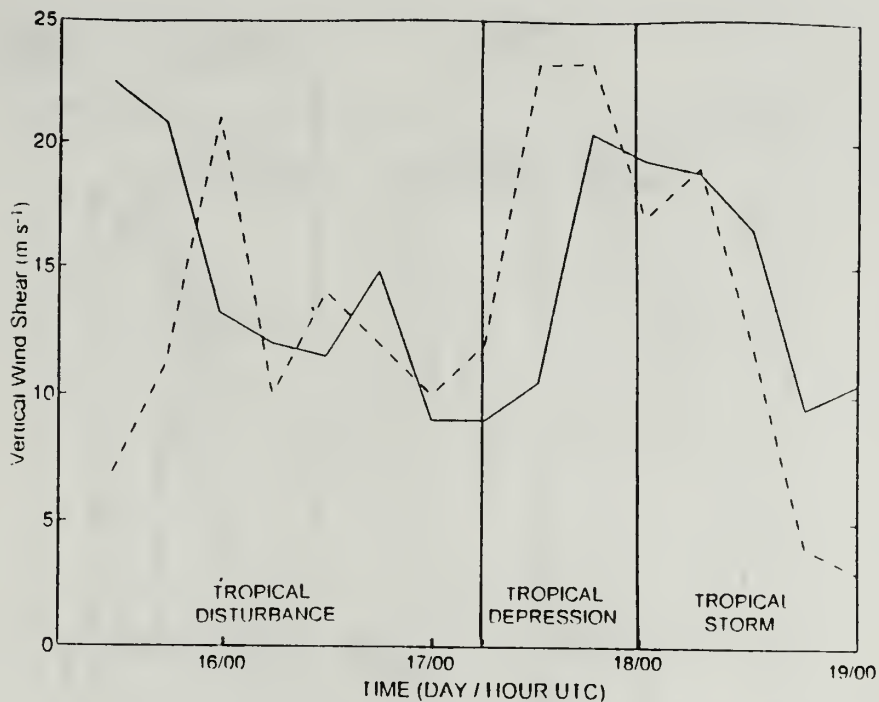


Figure 22. Vertical wind shear (m s^{-1}) over TC Zola from the TCM-90 analyses (solid) and over a ship (dashed) located between TC Zola and TC Yancy for 12 UTC 15 August to 00 UTC 19 August 1990 during each stage of TC Zola's development.

shear was decreasing (Fig. 23). Although the velocity then started to increase while the shear was increasing, the pre-Zola disturbance became a tropical depression when the shear had again decreased to 9 m s^{-1} . This is similar to the pre-Steve disturbance whose intensity remained nearly steady for most of the disturbance stage and then it increased under moderate to strong shear.

The final TCM-90 analyses (50 km resolution) were also used to calculate the 850/200 mb zonal vertical wind shear (not shown). The easterly shear over the pre-Zola disturbance was 20 m s^{-1} at 06 UTC 15 August and decreased to 15 m s^{-1} at 18 UTC 15 August. The shear pattern resembles the pattern of

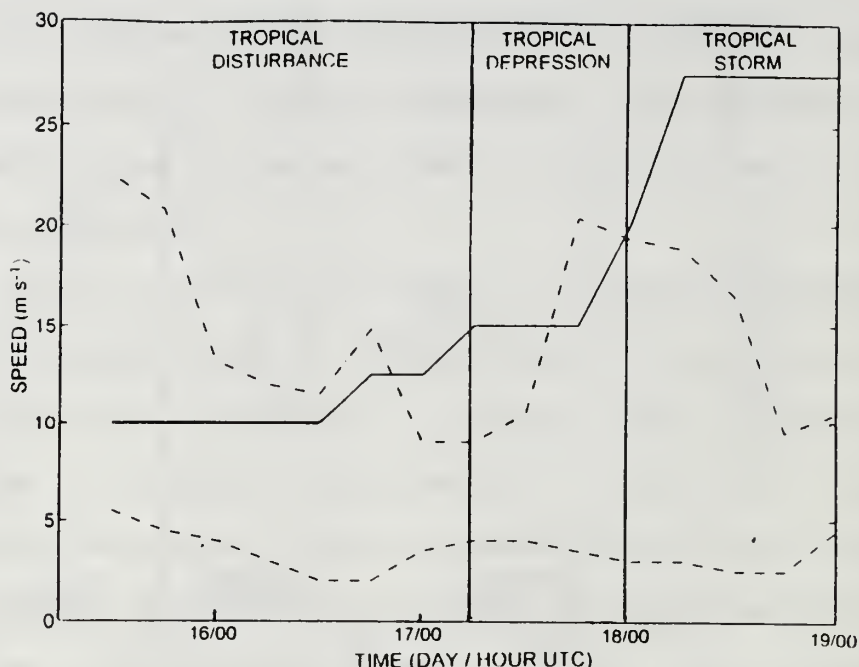


Figure 23. Low-level maximum velocity (intensity) of TC Zola (solid), 850/200 mb vertical wind shear (dot/dash), and translation speed (dashed) for 12 UTC 15 August to 00 UTC 19 August 1990.

McBride and Zehr (1981), with the large difference that the pre-Zola disturbance was not on the zero shear line, but was in an area of rather large easterly vertical shear. However, the shear did reduce to near zero at 18 UTC 16 August, and this may have been a key factor that allowed the disturbance to develop into a TD since all of Zehr's threshold values were then satisfied.

The EFC (Fig. 24) was positive near the center to 00 UTC 16 August, after which it became negative. From 750-1500 km, the EFC was negative at the beginning of the period but it became positive about mid period. The negative EFC would generate more anticyclonic flow which is detrimental to

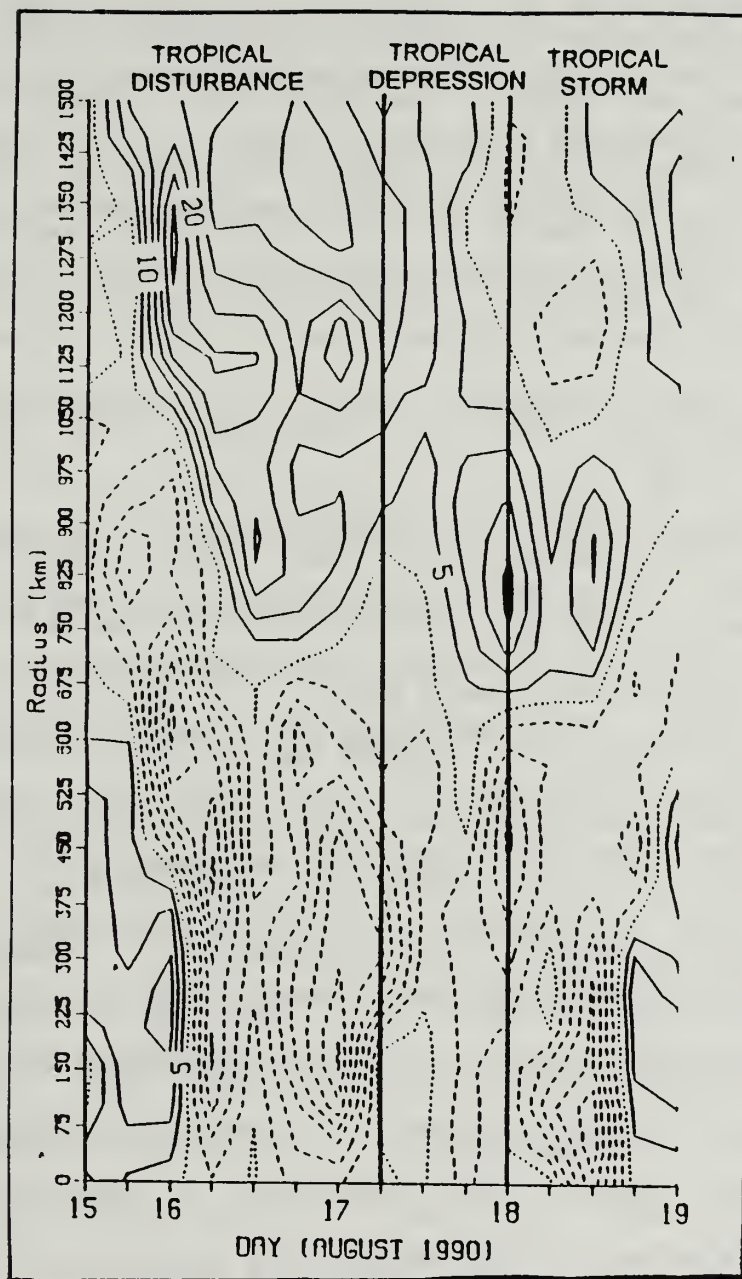


Figure 24. 200 mb Eddy Flux Convergence (EFC) (contour interval $3 \text{ m s}^{-1} \text{ d}^{-1}$) from 12 UTC 15 August to 00 UTC 19 August 1990 for TC Zola calculated from the TCM-90 analyses. Solid (dashed) lines represent increasing (decreasing) cyclonic tendencies.

development and intensification since it does increase upward motion (DeMaria et al. 1993). The negative EFC appears to be due to the point-source divergence located about 750 km to the east, which perhaps blocked the cyclonic influence of the TUTT (Fig. 19b). The point-source divergence moved to west of pre-Zola by 18 UTC 16 August (not shown), which allowed the TUTT to provide greater influence on the EFC. This differs from the pre-Steve disturbance stage in which the EFC was positive out to 1300 km.

In summary, pre-Zola formed closer to Typhoon Yancy (less than 10 deg. lat.) than would normally be expected. However, the upper-level outflow from the typhoon does not appear to be over pre-Zola. The moderate to strong vertical wind shear over pre-Zola appears to be due to the large-scale environment, with the magnitude decreasing by the end of the stage. This is consistent with the pre-Steve case in which the outflow from Robyn was constricted on the eastern side with the moderate shear over the disturbance being produced by the large-scale environment. Perhaps the constraints on the upper-level outflow are important to the development of a trailing system by decreasing the amount of shear over the formation area.

B. TROPICAL DEPRESSION STAGE (06 UTC 17 AUGUST TO 18 UTC 17 AUGUST)

The pre-Zola tropical disturbance was upgraded to a TD at 06 UTC 17 August. TD Zola was located east-southeast of Typhoon Yancy in the monsoon gyre and the intensity of Typhoon Yancy increased throughout the TD stage of Zola. TD Zola continued to move over a warm ocean, with the SST remaining at 30°C.

Since TD Zola continued to track north-northeastward throughout this stage at about 6 kt (Fig. 20), and Typhoon Yancy continued moving west-northwestward at 8 kt, the separation distance between the two systems increased from 15 deg. lat. to 18 deg. lat. This separation distance is equal to the mean distance for new system development in the wake of an existing TC (Briegel 1993). The larger separation distance means that the system was in an even more favorable location for development. The separation distance between Zola and Yancy was about 2 deg. lat. larger than for Steve and Robyn in the TD stage. This was a function of the spatial size of the leading system. The satellite imagery show that Typhoon Yancy appears to be larger (about 2-3 deg. lat.) than Typhoon Robyn, so a larger separation distance may have been needed between Yancy and Zola.

A low-level surge in the southwest monsoon flow into TD Zola occurred from 06 UTC to 18 UTC 17 August. At 850 mb (Fig. 25a), Zola was now a distinct circulation from Typhoon

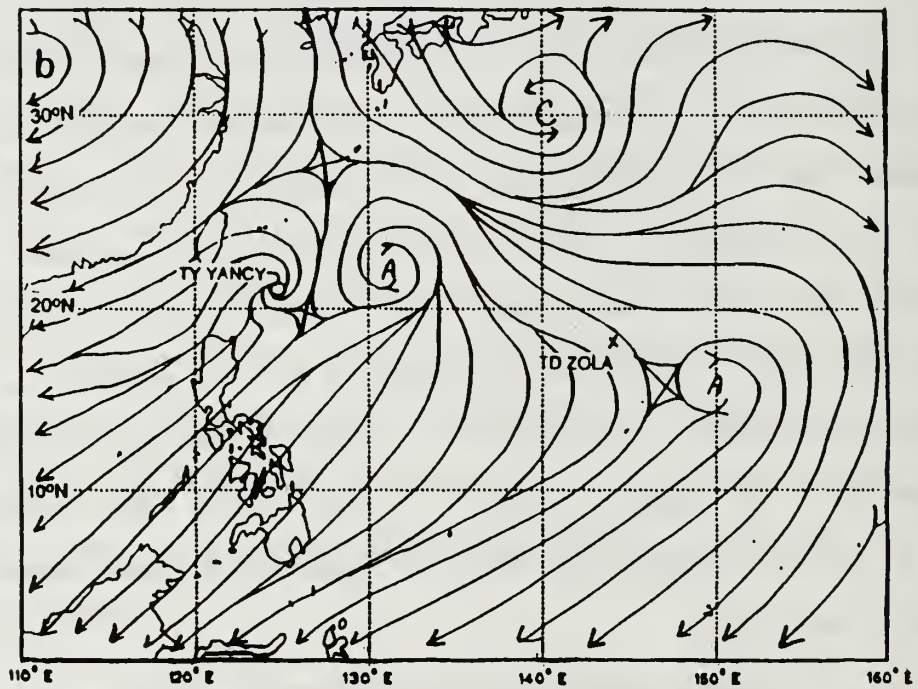
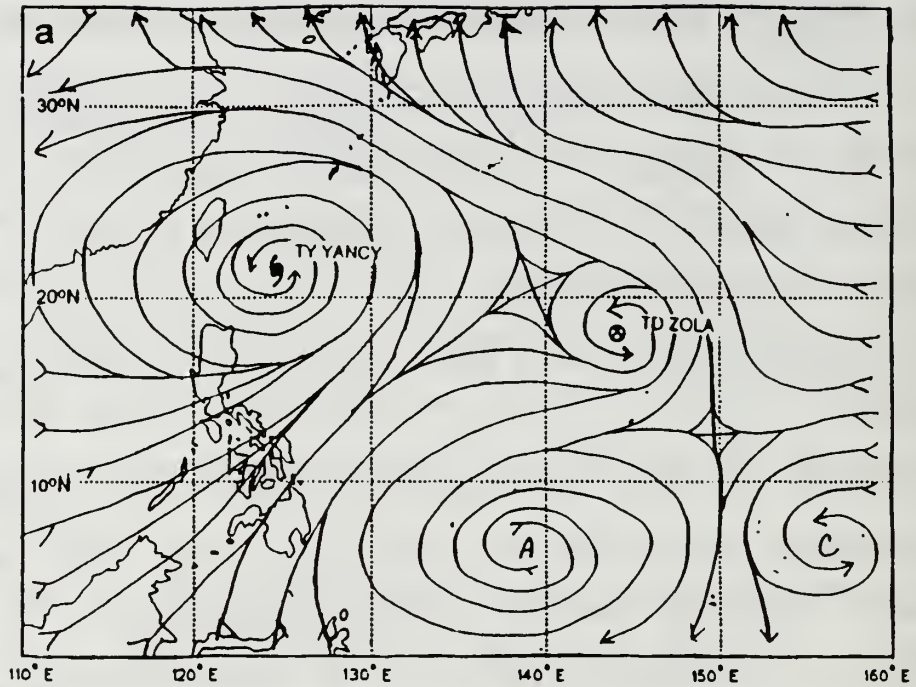


Figure 25. Streamline analyses over the western North Pacific for 18 UTC 17 August 1990 at (a) 850 mb and (b) 200 mb.

Yancy, and the cyclone over the South China Sea had filled. This pattern was again similar to the Rossby wave train dispersion schematic of Fig. 12b. The equatorial anticyclone was located south-southwest of TD Zola, which enhanced the monsoonal inflow into both Typhoon Yancy and TD Zola. The inflow to Zola also included a southeast to east flow along the southern edge of the subtropical ridge. The inflow regime to TD Zola is similar to that of TD Steve, but the surge that occurred into TD Steve was in the flow around the subtropical ridge vice an increase in the southwest monsoon.

At 200 mb (Fig. 25b), the TUTT cell had moved northeast to the base of a midlatitude trough at 18 UTC 17 August. The upper-level anticyclone trailing Typhoon Yancy tracked closer to the outflow area of Typhoon Yancy. After the TUTT cell started moving eastward with the midlatitude trough, the anticyclone then moved to a position more centered between Yancy and Zola. This is similar to the TD Steve case in which an upper-level anticyclone that developed due to the deep convection within the large outer circulation and inflow to Robyn was located at times between Robyn and Steve. This flow combined with Robyn's outflow and the TUTT to impinge on TD Steve. In this case, the northwesterly flow between the upper-level anticyclone and midlatitude trough/TUTT cell impinged on Zola. Thus, the vertical wind shear generated over TD Zola was due to the flow between the anticyclone and the TUTT cell, with Typhoon Yancy providing a weak

contribution. A southwest outflow channel for TD Zola developed near the end of the period.

The vertical wind shear over TD Zola (Fig. 22) was less than Zehr's (1992) value of 12.5 m s^{-1} early in the TD stage, but increased significantly at the end of the stage. This is supported by the vertical wind shear calculated from upper air soundings from two ships. The first ship (Fig. 22), which was located near 19°N , 131°E , had an earlier increase in wind shear. The second ship (not shown) located near 19°N , 140°E recorded a 23.2 m s^{-1} vertical wind shear from 12 UTC - 18 UTC 17 August. Thus, TD Zola came under strong vertical wind shear at the end of the TD stage. This is also similar to the TD stage for TC Steve, in which the vertical wind shear was less than Zehr's threshold shear value until the end of the stage. The vertical wind shear is primarily caused by the upper-level flow between the anticyclone and TUTT cell and not due to the outflow from Typhoon Yancy (Fig. 25b). For Steve, the outflow from Typhoon Robyn contributed to the vertical shear over Steve, but the primary contributors were also the upper-level anticyclone and the TUTT.

The intensity remained steady from the beginning of the TD stage until 18 UTC 17 August (Fig. 23), even though the shear was below Zehr's threshold value. The subsequent increase in intensity occurred under strong shear conditions (Fig. 23). This is similar to the TD Steve case, although TD Steve

increased in intensity under increasing shear throughout its TD stage.

EFC was negative from the center to 675 km for the entire TD stage. This appears to be due to the location of TD Zola under the anticyclonic flow around an anticyclone to the southeast of TD Zola (Fig. 25b). According to DeMaria et al. (1993), this would not be conducive for development of the TC since it would decrease upward vertical motion. By contrast, the EFC for TD Steve was positive at the beginning of the TD stage and only became negative near the end of the stage.

The LLCC was displaced from the deep convection, due to the strong vertical wind shear that was impinging on the northwestern side of TD Zola. Unfortunately, few high-resolution satellite images are available for this TD stage. Two enhanced IR images on 17 August show the location of deep convection in TD Zola. The first image (Fig. 26) at 1132 UTC (2132 local) has the deepest convection over the center and southward to the southern edge of the partially exposed LLCC. Thus, only the northern half of the LLCC was exposed. In the second image (Fig. 27) at 1732 UTC (0742 local, during the convective maximum period) the LLCC was fully covered with the coldest cloud tops southwest of the vortex center. The location of the coldest cloud tops for the exposed LLCC in TD Zola was similar to that found with TD Steve. The pattern is similar to the schematic with forced descent over the edge of the LLCC (Fig. 17b). Thus, the circulation of the latent heat

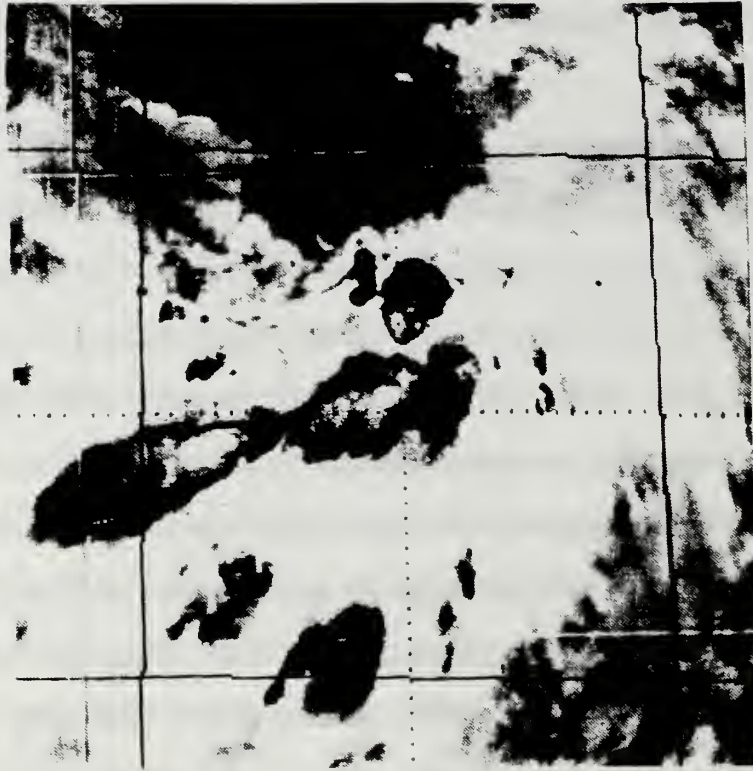


Figure 26. IR satellite imagery for 1132 UTC 17 August 1990 showing the partial exposure of the LLCC for TD Zola with the coldest cloud tops located over the southern edge of the LLCC.

released in the deepest convection may have aided the TD Zola system in maintaining a warm core and in resisting the vertical wind shear that exposed the LLCC. After 18 UTC 17 August it also had to be strong enough to lower the surface pressure, and increase the intensity of the system.

The 850 mb relative vorticity and divergence (Fig. 21) continued to exceed the threshold values of Zehr (1992). Anticyclone relative vorticity and divergence were calculated at 200 mb (not shown). The radiosondes from the islands listed in the disturbance stage indicate that moisture (dewpoint depression $< 5^{\circ}\text{C}$) was available up to at least 400

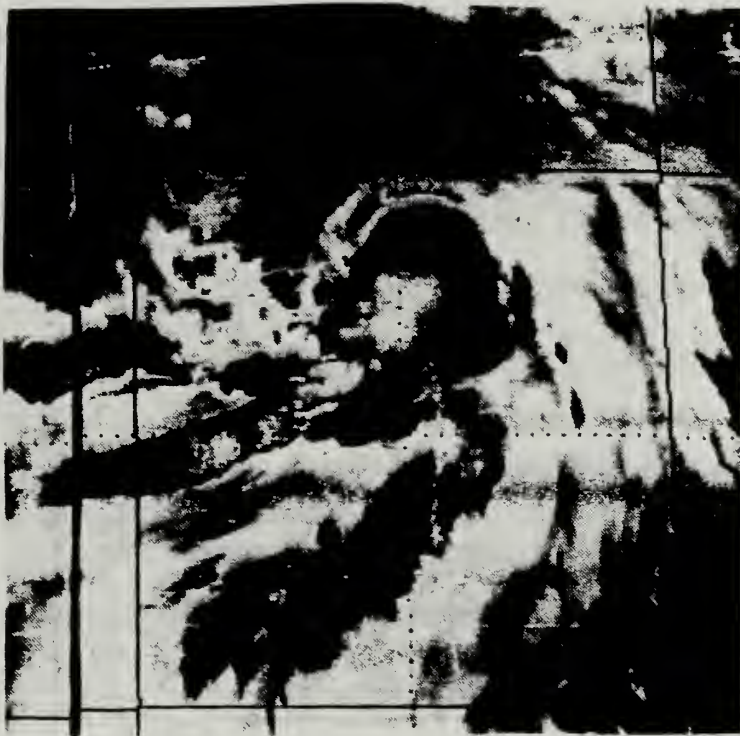


Figure 27. IR satellite imagery for 1732 UTC 17 August 1990 showing the recovered LLCC of TD Zola with the coldest cloud tops located near the center and to the southwest portion of the LLCC.

mb in the inflow to TD Zola. With the exception of vertical wind shear, the environmental conditions were conducive for TC development.

C. TROPICAL STORM STAGE (00 UTC 18 AUGUST TO 00 UTC 19 AUGUST)

Since the maximum velocity of TD Zola evidently increased to 40 kt at 00 UTC 18 August, TD Zola should have been upgraded to a TS. However, JTWC did not officially upgrade TD Zola until after the receipt of a ship report of 55 kt and a 998 mb sea-level pressure (ATCR 1990). The official maximum

velocity of Zola then increased another 15 kt at 06 UTC 18 August to 55 kt.

At 850 mb (Fig. 28a), TS Zola had broken away from the monsoon gyre by 12 UTC 18 August. The subtropical ridge built westward and combined with a dynamic high that moved off the coast of China to Japan. At 12 UTC 18 August, Zola started moving northwestward under the influence an enhanced pressure gradient between Yancy and the subtropical ridge cell to the east, which may account for the rapid rate of recurvature of Zola (Fig. 20). The equatorial anticyclone southwest of Zola and the cyclone southeast of Zola combined to produce southerly inflow to Zola. This differs slightly from the TS Steve case, in which the equatorial anticyclone maintained a position southeast of Steve, with southwesterly winds dominating the inflow to Steve.

At 200 mb (Fig. 28b), the northwesterly flow between the midlatitude trough and the anticyclone trailing Yancy continued to impinge on and be deflected by the outflow from Zola. Zola still had a good southwestward outflow channel. This is similar to the Steve case, which also had an impinging northeasterly flow, which created the bow-wave effect around Steve and a good outflow channel to the southwest.

The 850-200 mb vertical wind shear (Fig. 22) remained large early in the TS stage, then it decreased to less than Zehr's threshold value at 18 UTC 18 August. This is also supported by upper-air soundings taken by a ship near 20°N,

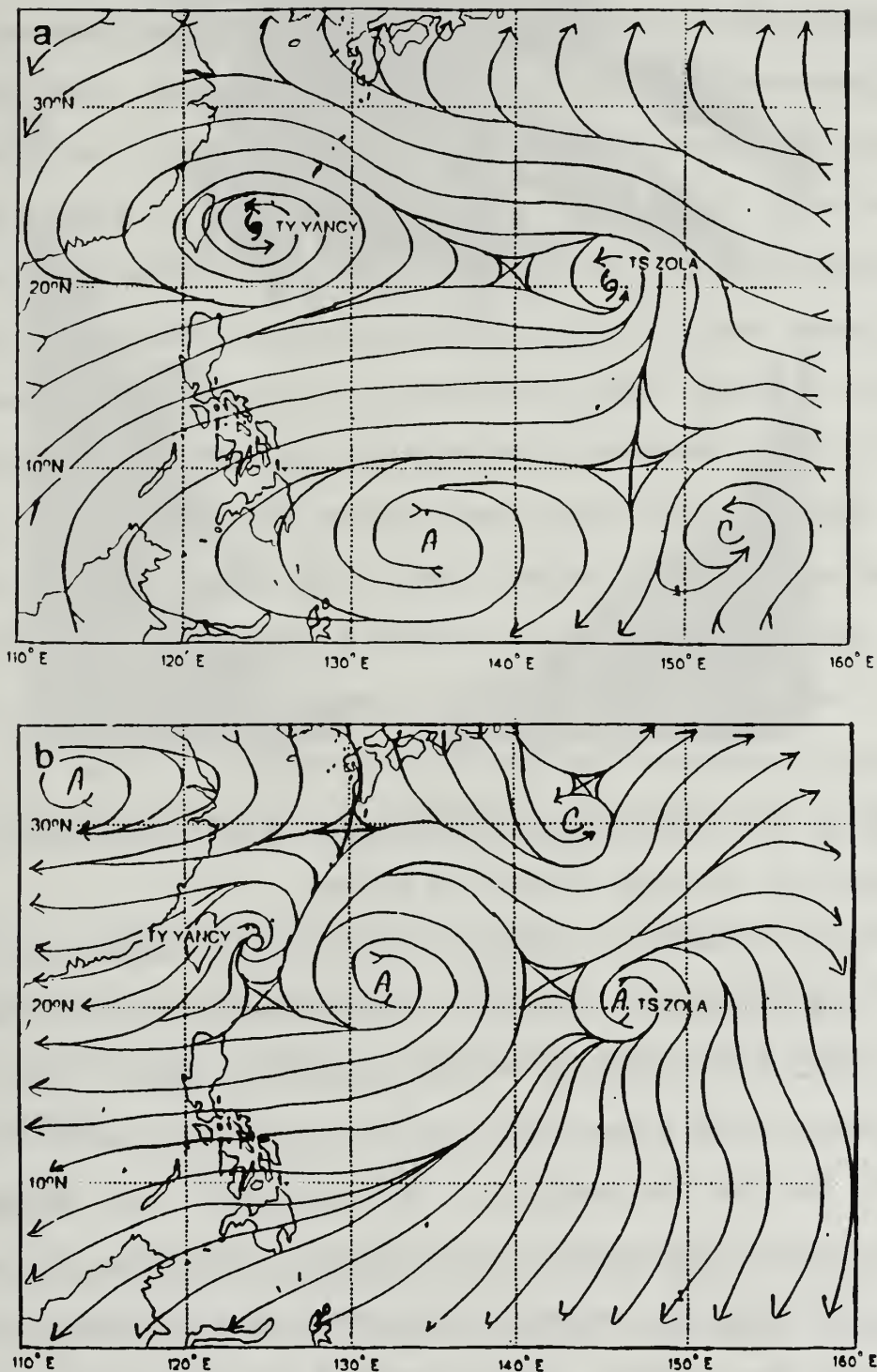


Figure 28. Streamline analyses over the western North Pacific for 12 UTC 18 August 1990 at (a) 850 mb, and (b) 200 mb.

131°E (Fig. 22), except the wind shear decreased to lower values than over TS Zola. This corresponds well to the exposure of the LLCC in satellite imagery. The decrease in vertical wind shear is correlated with an increase in intensity (Fig. 23) at the beginning of this stage. The intensification of the storm indicates that the outflow was stronger and thus, more effective in "fighting off the shear." This differs from TS Steve, in that the analyses do not accurately document the decrease in vertical wind shear over TS Steve. This decrease occurs for this case due to the development of an upper-level anticyclone over TS Zola.

Although the EFC for TS Zola (Fig. 26) was negative near the center at the beginning the TS stage, a weak positive signal developed at 18 UTC 18 August. This is basically similar to TS Steve, where positive EFC developed near the center at the end of the TS stage.

Only a few high-resolution satellite images were available for the TS stage. The LLCC was almost completely exposed in the 0503 UTC 18 August visual satellite image (Fig. 29). The coldest cloud tops were over the south-southeast edge of the LLCC in the IR imagery. As discussed for TC Steve, the location of the coldest cloud tops on the edge of the LLCC may have allowed air warmed from latent heat release to circulate around the vortex, which helped maintain the warm core, similar to the schematic in Fig. 17a. The LLCC was then covered in the IR image of 1832 UTC (0432 local diurnal

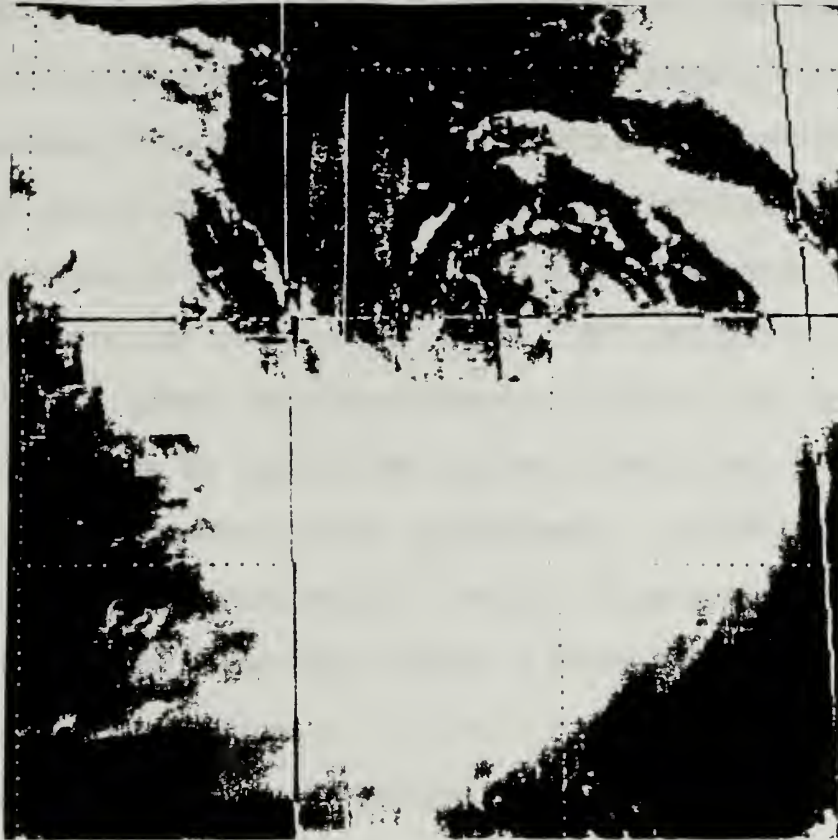


Figure 29. Visible satellite imagery for 0530 UTC 18 August 1990 showing the almost completely exposed LLCC of TS Zola.

maximum) 18 August (not shown) and was not exposed in any of the remainder of the imagery. That is, the effects of the vertical wind shear appear to have been negligible after 1832 UTC 18 August:

D. SUMMARY

TUTT-associated divergence aided in the early development of both Zola and Steve. Zola initially formed closer to Typhoon Yancy (8 deg. lat.) than Steve formed near Typhoon Robyn (11.9 deg. lat.). The systems appear to have developed

close to the leading typhoon because the upper-level outflow was restricted on the eastern side, and thus could not contribute to the shear over the formation areas. As in the Steve case, the vertical wind shear over the development area was not primarily due to the outflow of the nearby typhoon but rather to the TUTT and other environmental influences. Although the leading typhoon did generate a portion of the vertical wind shear during the TD and TS stages, this was not the only effect. Generally, the flow between a TUTT and an anticyclone couplet that trailed the leading typhoon was responsible for much of the vertical wind shear over the developing system.

The effects of the strong vertical wind shear can be collaborated by the exposure of the LLCC in the satellite imagery. Nevertheless, Zola increased in intensity under moderate to strong shear. The limited amount of satellite imagery for Zola indicated the location of the coldest cloud tops was similar to that in the TC Steve case. This asymmetry aided in maintenance of Zola against the inhibiting effects of the vertical wind shear and assisted in increasing the intensity. The model (Fig. 17) that was discussed for the TC Steve case appears to be valid for TC Zola.

The EFC did not play a role in the intensification of TC Zola since it was negative near the center for almost the entire case. This indicates that anticyclonic flow over the center would try to reduce the upward vertical motion and tend

to inhibit development and intensification. This was also the case for two periods during the TC Steve case.

A low-level surge that occurred in the TD stage of Zola is similar to the surge that occurred in the disturbance stage of the TC Steve case. The Rossby wave train schematic (Fig. 12b) with a pattern of a monsoon gyre and anticyclone to the southeast and the trailing TC developing north of the anticyclone seems to apply for both this case and the TC Steve case. The low-level surge appears to be related to the development of the Rossby wave trough to the east-southeast of the leading TC and the surge leads to an increase in low-level convergence. For TC Steve, a second low-level surge from the east-southeast also occurred during the TD stage.

VI. TROPICAL CYCLONE OMAR

A. TROPICAL DISTURBANCE STAGE (06 UTC 20 AUGUST TO 18 UTC 23 AUGUST)

The pre-Omar disturbance was detected as an area of persistent convection over the southern Marshall Islands. The pre-Omar disturbance formed in the flow around the southern edge of the subtropical ridge. This pre-Omar disturbance existed for more than three days before the disturbance that developed into Polly appeared just west of Guam at 12 UTC 23 August. Thus, this case differs considerably from the Steve and Zola cases, in which the leading systems (Robyn and Yancy) were already at tropical storm strength when Steve and Zola developed. Whereas, Steve and Zola were under significant vertical wind shear from the beginning, the vertical wind shear for Omar did not become an important factor until it had reached tropical storm intensity.

The tracks of pre-Omar and pre-Polly are shown in Fig. 30. Both disturbances tracked west-northwest at an average speed of 10 kt under the influence of the east-southeasterly winds along the southern edge of the subtropical ridge. Pre-Polly formed about 16 deg. lat. west-northwest of pre-Omar and this separation distance did not increase during the remainder of this stage.

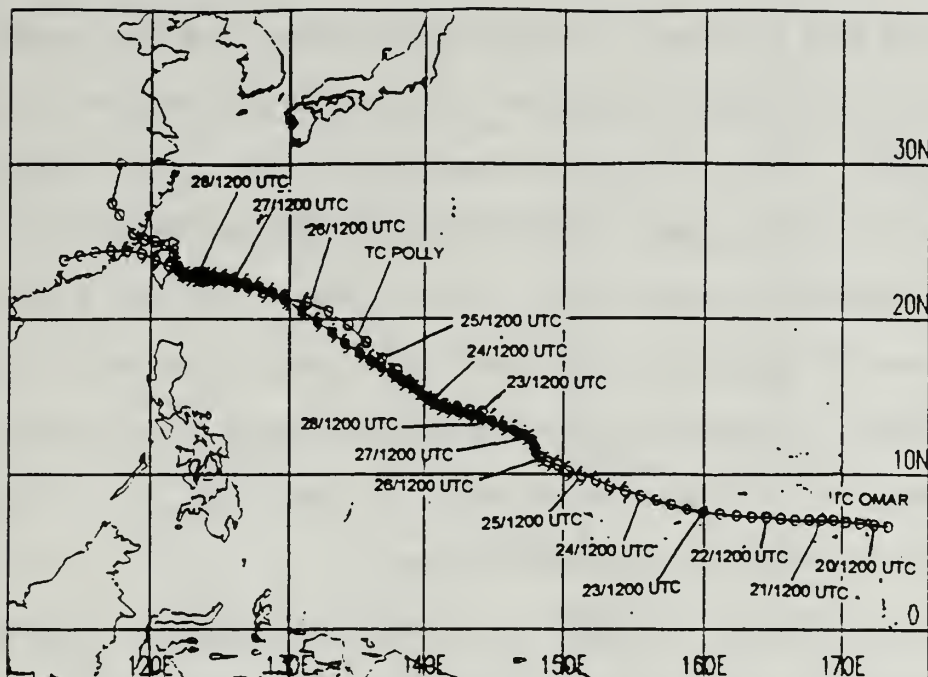


Figure 30. JTWC best tracks for TC Omar and TC Polly during August 1992 with symbols as in Fig. 3.

The JTWC hand-drawn analyses for surface/gradient level and 200 mb were used in this case. The multi-quadric 850 mb and 200 mb analyses were in good agreement with the JTWC analyses concerning the location of the centers and the overall flow patterns. The multi-quadric analyses were used to calculate the vertical wind shear, zonal wind shear, relative vorticity, convergence, and EFC of angular momentum.

During the beginning of this stage (maps not shown), the monsoon trough extended eastward from China to TS Lois east of Japan. Although a monsoon gyre was located south of Guam, ridging dominated the normal position of the monsoon trough for this time of year. Omar and Polly developed during a major relocation of the monsoon trough to a position extending

across the northern Philippine Islands and east-southeastward into the Caroline Islands. Pre-Polly formed as the southwest monsoon flow intensified westward over its formation area. When pre-Polly was detected, both storms were located within the monsoon trough (Fig. 31a). Pre-Polly was located within a monsoon gyre and pre-Omar was associated with a low-level cyclone. This slightly differed from the Steve and Zola cases, in which the monsoon trough was in a more normal position when the systems formed.

At 200 mb, a TUTT cell was northeast of the pre-Omar disturbance at 12 UTC 20 August. The TUTT cell and the TUTT axis shifted farther northward with divergent flow forming over the pre-Omar disturbance area on 00 UTC 22 August (not shown). An upper-level anticyclone then developed with pre-Omar located underneath the divergent outflow (Fig. 31b). Weak TUTT-associated divergence was over pre-Polly throughout the disturbance period, which was also the case for Steve and Zola. Near the end of this stage, a TUTT cell north of the pre-Polly disturbance remained and the major TUTT axis shifted southeastward (Fig. 31b). An anticyclone then developed to the southwest of the pre-Polly disturbance.

The vertical wind shear over the pre-Omar disturbance remained less than Zehr's (1992) threshold of 12.5 m s^{-1} (Fig. 32). Thus, the vertical wind shear for this stage of pre-Omar was smaller than for TC Steve and TC Zola disturbance stages. A decrease occurred from 00 UTC 23 August to 00 UTC 24 August,

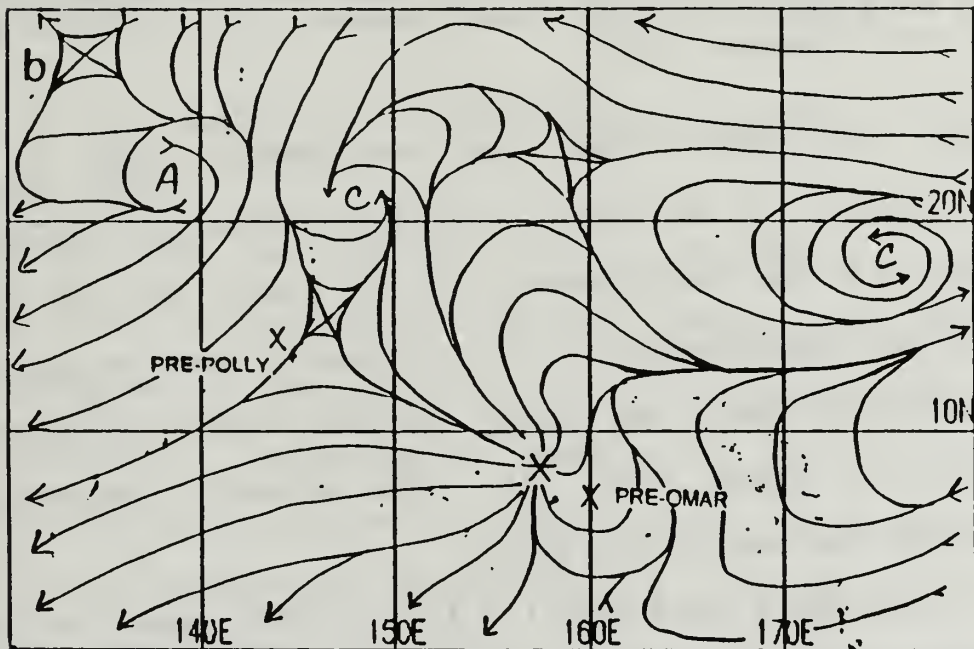
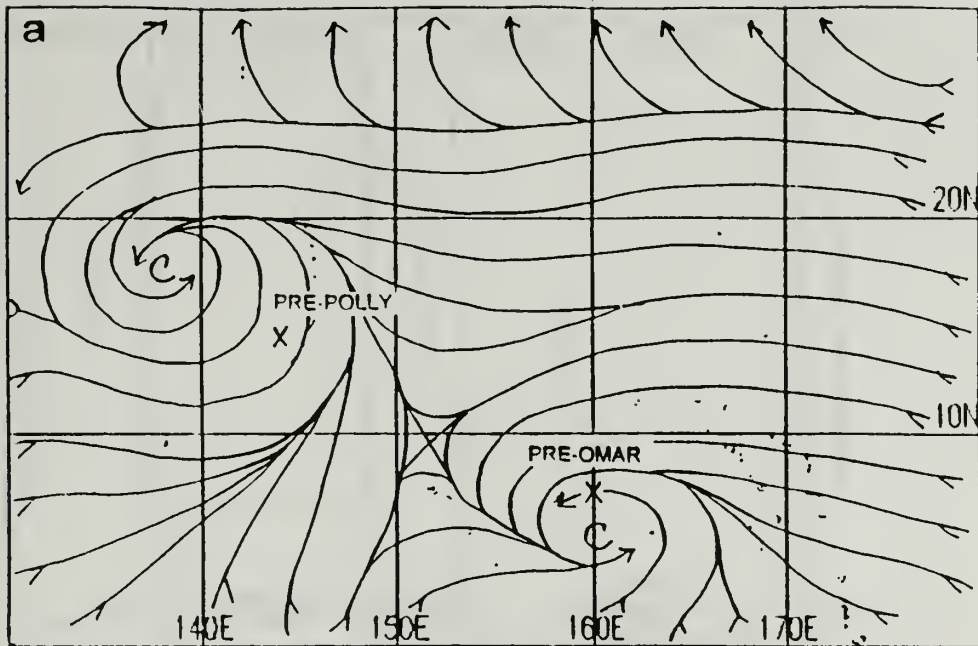


Figure 31. Streamline analyses over the western North Pacific for 12 UTC 23 August 1992 at (a) surface/gradient level, and (b) 200 mb.

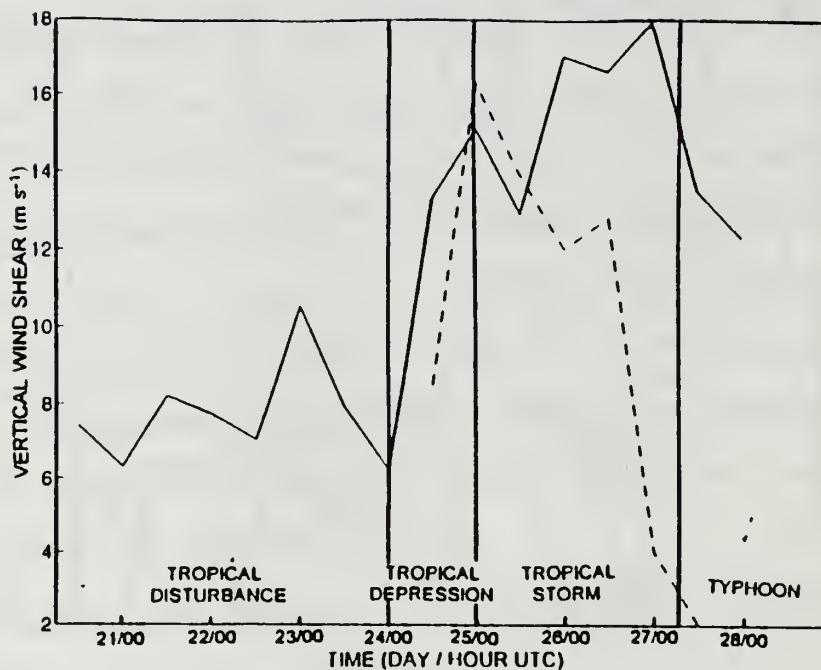


Figure 32. Vertical wind shear (m s^{-1}) over TC Omar from the multi-quadric analyses (solid) for 12 UTC 20 August 1990 to 00 UTC 28 August, and over Guam (dashed) for 12 UTC 24 August to 12 UTC 27 August 1992.

which was just after the development into a tropical depression. A decrease in vertical shear also occurred just prior to the development of TC Steve and TC Zola into tropical depressions. The intensity was steady and the translation speed was nearly constant under the shear through 12 UTC 22 August (Fig. 33). The intensity increased slowly through the end of the stage.

Pre-Omar formed near the line of zero zonal vertical wind shear separating the easterly and westerly shear (not shown), which was an indication that pre-Omar was moving into a favorable environment. These shears remained less than 10 m s^{-1} over pre-Omar for the entire stage. This arrangement of

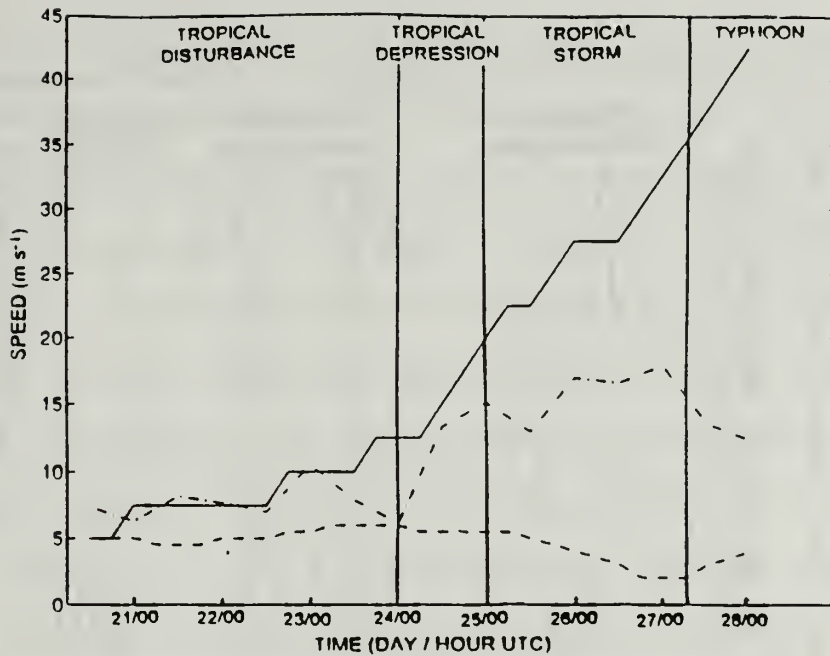


Figure 33. Low-level maximum velocity (intensity) of TC Omar (solid), 850/200 mb vertical wind shear (dot/dash), and translation speed (dashed) for 06 UTC 20 August to 00 UTC 28 August 1992.

shear is also conducive for development according to McBride and Zehr (1981).

The EFC (Fig. 34) was positive from the center to 1500 km for the first 36 h and then it became negative. The negative EFC corresponds to the ridging that built over pre-Omar by 00 UTC 22 August. According to DeMaria et al. (1993), the positive EFC is conducive to formation and the negative EFC would not be considered conducive since it would not work to increase upward vertical motion. The low-level influx of moisture and convergence into pre-Omar and pre-Zola could have produced significant upward motion so that the inhibiting effects of the negative EFC were offset.

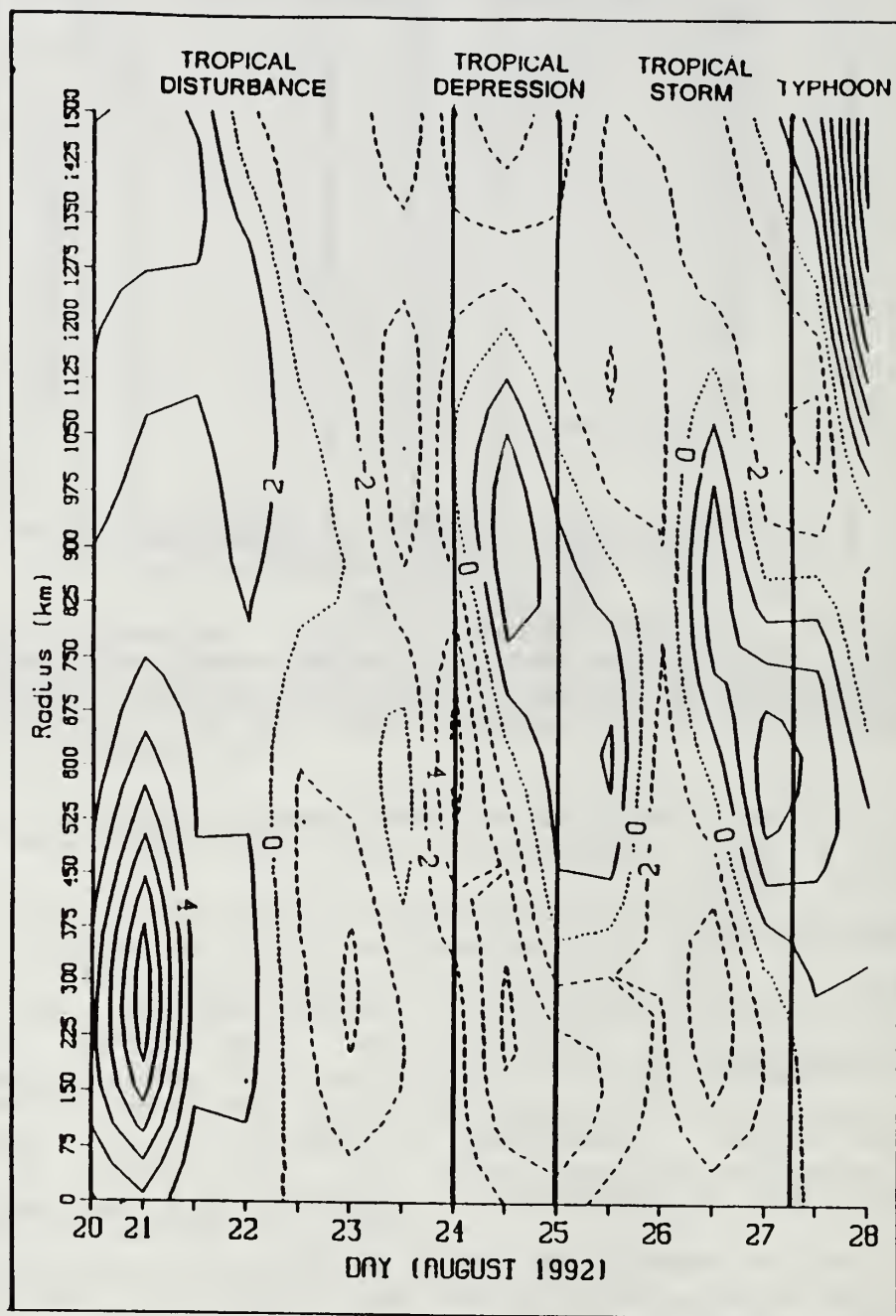


Figure 34. 200 mb Eddy Flux Convergence (EFC) (contour interval $2 \text{ m s}^{-1} \text{ d}^{-1}$) from 12 UTC 20 August to 00 UTC 28 August 1992 for TC Omar calculated from the multi-quadric analyses. Solid (dashed) lines represent increasing (decreasing) cyclonic tendencies.

Satellite imagery for this period was limited. An MCV in the pre-Omar circulation was detected during the diurnal convective minimum on 23 August. This is similar to the Steve case. As stated earlier, an MCV is conducive to development because it is a localized area of maximum relative vorticity. Pre-Omar had a more organized cloud signature than pre-Polly. Even though pre-Omar and pre-Polly were tropical disturbances, it was expected that the cloud top temperatures for pre-Omar would be lower since the disturbance had existed longer and the associated low-level convergence should be greater due to the MCV. Although the cloud top temperatures were similar (within 2-4°C) for both disturbances, pre-Omar generally had the colder cloud tops (Fig. 35), which also extended over a larger area. Thus, the deepest convection in both disturbances was almost equally deep, which was also the case for TC Steve and Typhoon Robyn.

The 850 mb relative vorticity and convergence (Fig. 36) over the pre-Omar disturbance met the requirements of Zehr, which were given in Chapter IV. Pre-Omar formed over SSTs greater than 29°C, which exceeds the required minimum of 26.5°C. Rawinsondes at two island stations, Ponape (7.0°N, 158.2°E) located to the southwest and Ailinglapalap (7.0°N, 171.2°E) to the southeast of pre-Omar, had moisture available up to 400 mb (not shown). Thus, all the preconditions for development of a TC were present when pre-Omar formed.

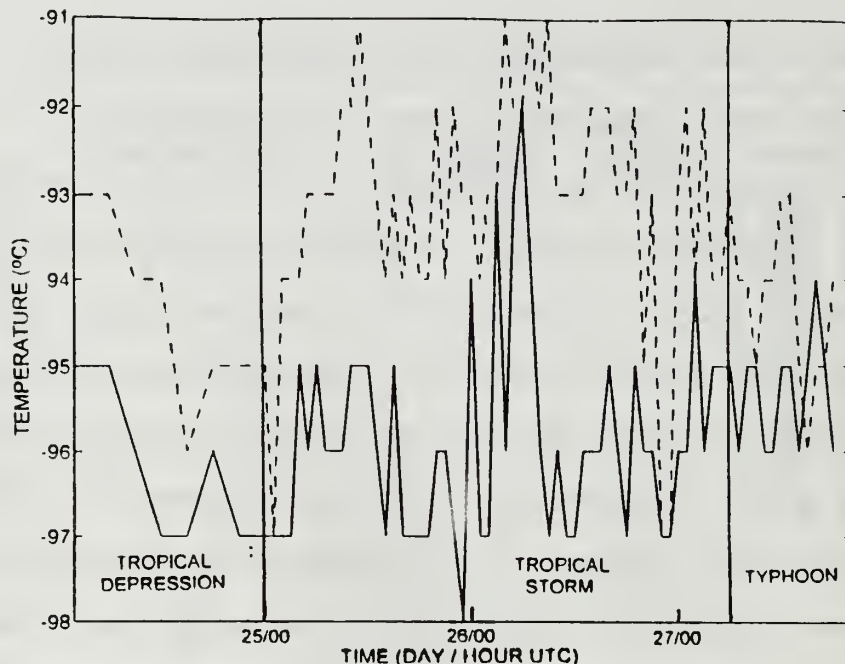


Figure 35. Minimum cloud top temperatures ($^{\circ}\text{C}$) from IR satellite imagery for TC Omar (solid) and TC Polly (dashed) for 0230 UTC 24 August to 1830 UTC 27 August 1992.

B. TROPICAL DEPRESSION STAGE (00 UTC 24 AUGUST TO 18 UTC 24 AUGUST)

The pre-Omar disturbance developed into a TD at 00 UTC 24 August when the maximum sustained winds increased to 25 kt. Since TD Omar moved west-northwest at 11 kt and pre-Polly moved west-northwest at 9 kt, the separation distance decreased slightly to 15.5 deg. lat. (Fig. 30). Both systems continued to track in the flow around the southern edge of the subtropical ridge.

At the surface/gradient level (Fig. 37a), pre-Polly was now associated with a surface cyclone. Good cross-equatorial flow existed for both storms. Low-level ridging was

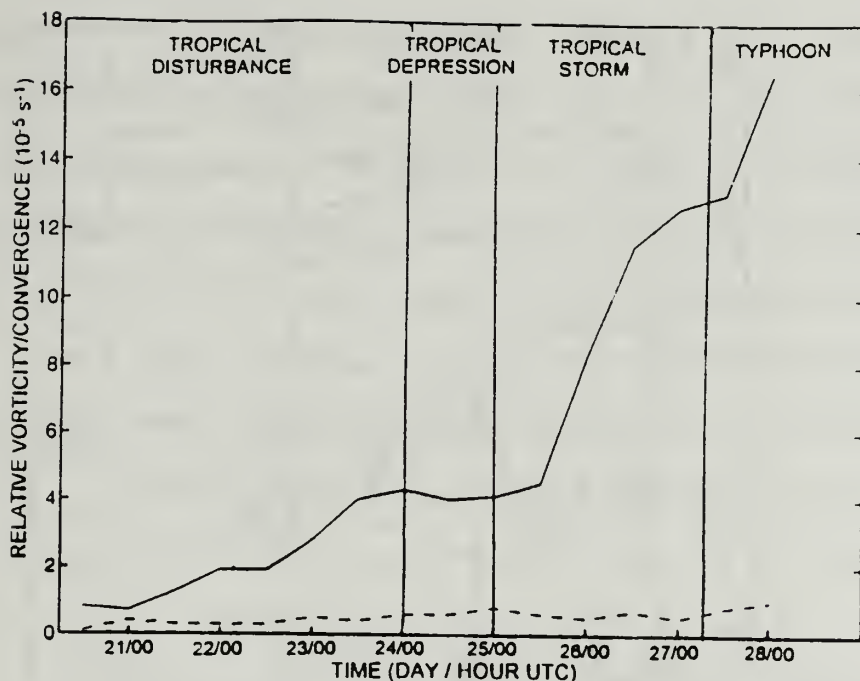


Figure 36. Relative vorticity (solid, 10^{-5} s^{-1}) and convergence (dashed, 10^{-5} s^{-1}) at 850 mb over TC Omar from 12 UTC 20 August to 00 UTC 28 August 1992 calculated from the multi-quadric analyses.

developing between the storms, which caused a break in the monsoon trough in which the storms were located. This ridging appeared to be the low-level response to subsidence occurring in a TUTT cell at upper levels between the two storms (Fig. 37b). This TUTT cell was between an anticyclone that had formed over TD Omar and another anticyclone east of Pre-Polly. This TUTT cell was at the west end of the main TUTT axis that extended northeastward.

The intensity of TD Omar increased steadily throughout this TD stage with the maximum wind speed increasing about 5 kt every 6 hours (Fig. 33). However, the vertical wind shear over TD Omar also increased through the period, and this was

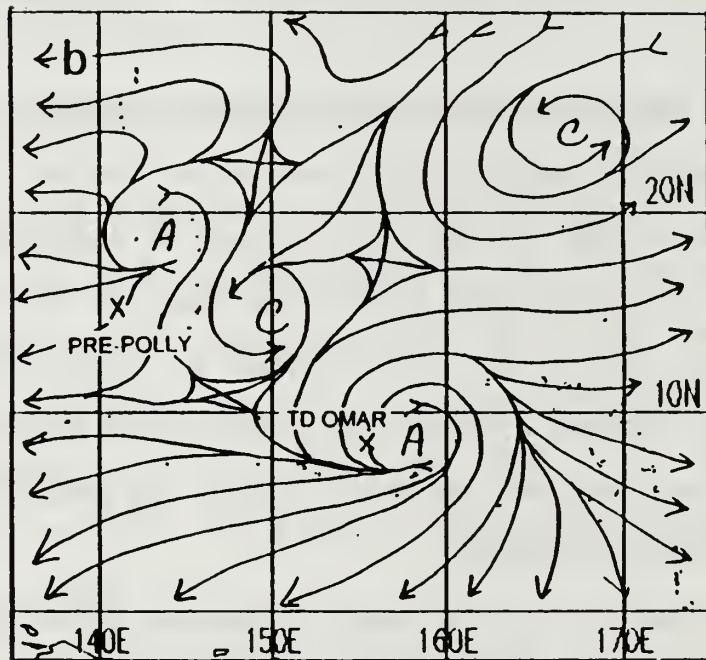
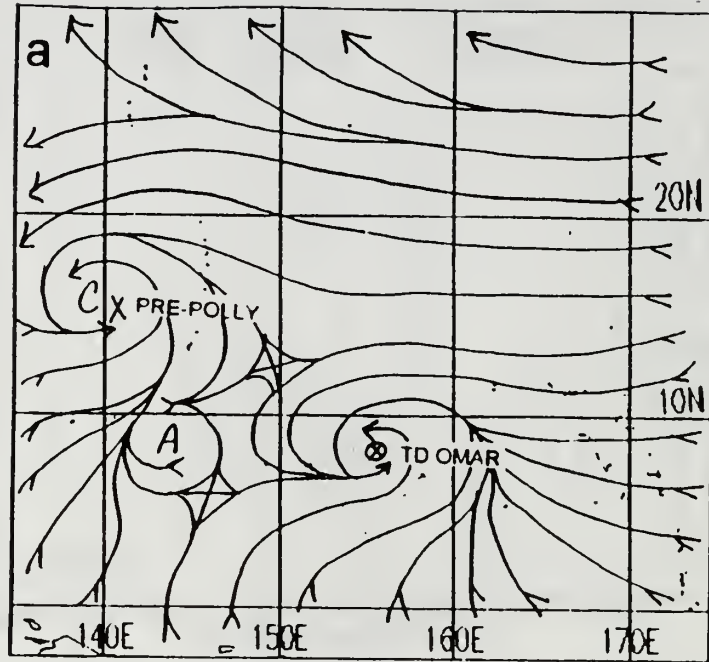


Figure 37. Streamline analyses over the western North Pacific for 12 UTC 24 August 1992 at (a) surface/gradient level, and (b) 200 mb.

confirmed by the soundings at Guam (Fig. 32). The shear calculated from the soundings were very similar (within 3 m s^{-1}) to the magnitude of the shear over Guam calculated using the multi-quadric analyses. In particular, the vertical wind shear now exceeding the 12.5 m s^{-1} threshold specified by Zehr (1992). This development, and subsequent intensification, therefore occurred under moderate shear as in the Steve and Zola cases. The EFC (Fig. 36) remained negative within 300 km of the center and this could be due to upper-level anticyclonic flow over TD Omar (Fig. 37b).

Satellite imagery available for this stage revealed that pre-Polly developed quickly into a large circulation so that it had a size comparable to TD Omar by the end of this stage. The coldest cloud tops in each system were similar (Fig. 35) with little diurnal variation. This differs from the Steve case where minimum cloud top temperature for Steve underwent a minor diurnal variation. Thus, the depths of the deepest convection were similar. However, Polly did not develop a core of persistent central convection. Deep convection encircled the vortex and was located with the inflow. Whereas the leading storms in the Steve and Zola cases were well-developed typhoons, Polly never became well organized.

The 850 mb relative vorticity and convergence (Fig. 36) still exceeded development thresholds. SST was approximately 29°C . Moisture was available up to 500 - 400 mb. Conditions

remained favorable for development, with the exception of vertical wind shear.

C. TROPICAL STORM STAGE (00 UTC 25 AUGUST TO 00 UTC 27 AUGUST)

TD Omar was upgraded to a TS at 00 UTC 25 August. The pre-Polly disturbance was upgraded to TD at 12 UTC 25 August and upgraded to a tropical storm at 12 UTC 26 August. Both systems tracked west-northwestward (Fig. 30). Omar moved at 10-12 kt until it started slowing down at 12 UTC 25 August due the ridging ahead of its location. Early in this stage, the separation between the storms remained at about 15 deg. lat. as both storms moved in the steering flow around the subtropical ridge. The distance between the storms increased from 16.5 to 21.5 deg. lat. between 12 UTC 26 August and 00 UTC 27 August as TS Polly continued to track west-northwestward at 16 kt while Omar drifted northwestward at 4 kt.

At the surface/gradient level (Fig. 38a), TD Polly was now at the center of a large monsoon gyre and the weak ridging was building southwestward between the storms. This ridging resulted from Rossby wave energy dispersion from the monsoon gyre in which Polly was embedded. The anticyclone in the Rossby wave train that a monsoon gyre generates generally forms to the southeast of the monsoon gyre in the northern West Pacific. Animated satellite imagery (Fig. 39) showed

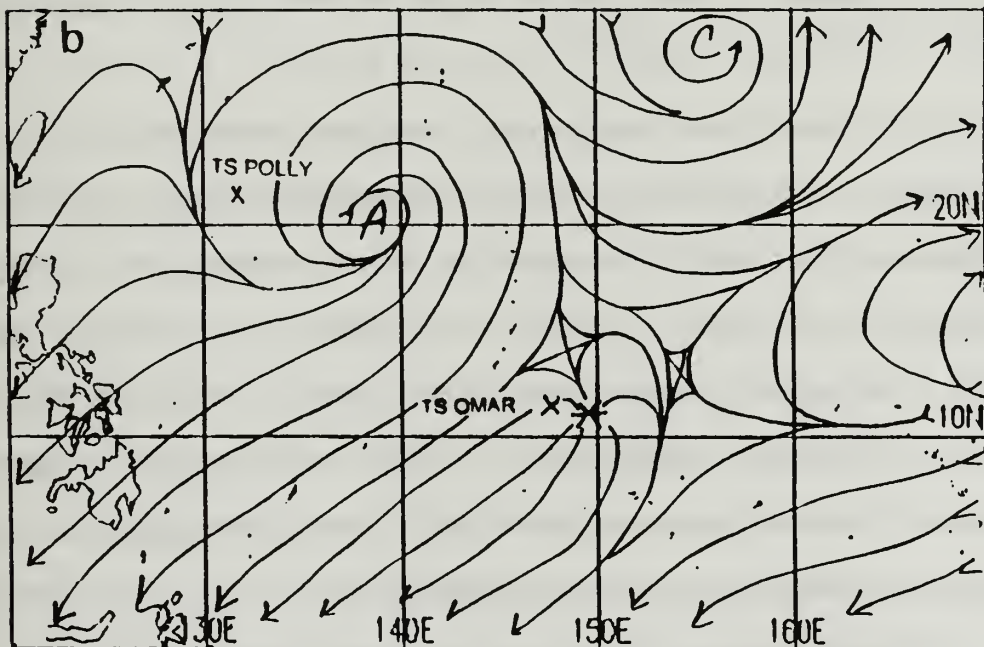
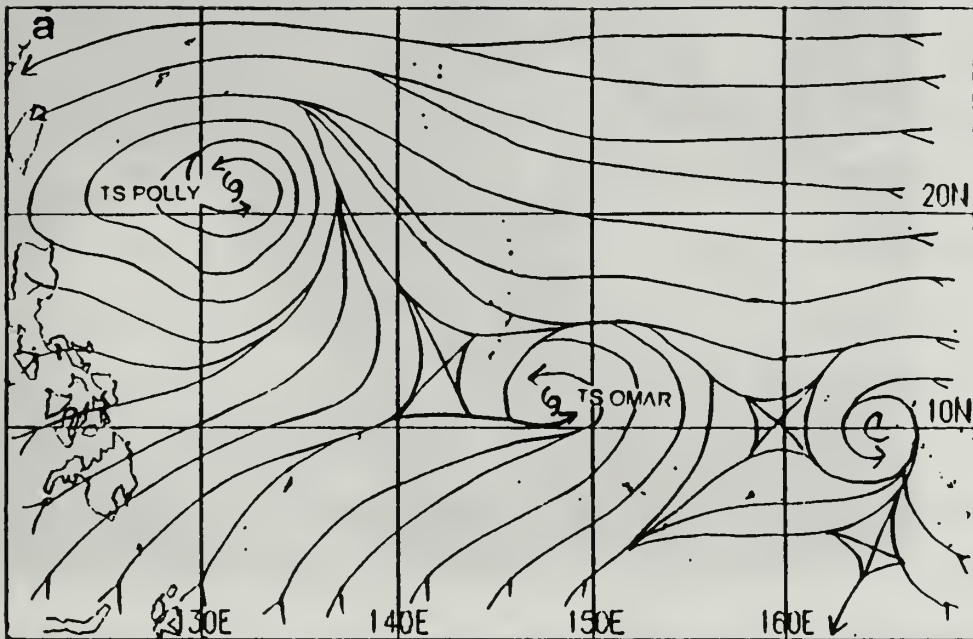


Figure 38. Streamline analyses over the western North Pacific for 12 UTC 26 August 1992 at (a) surface/gradient level, and (b) 200 mb.

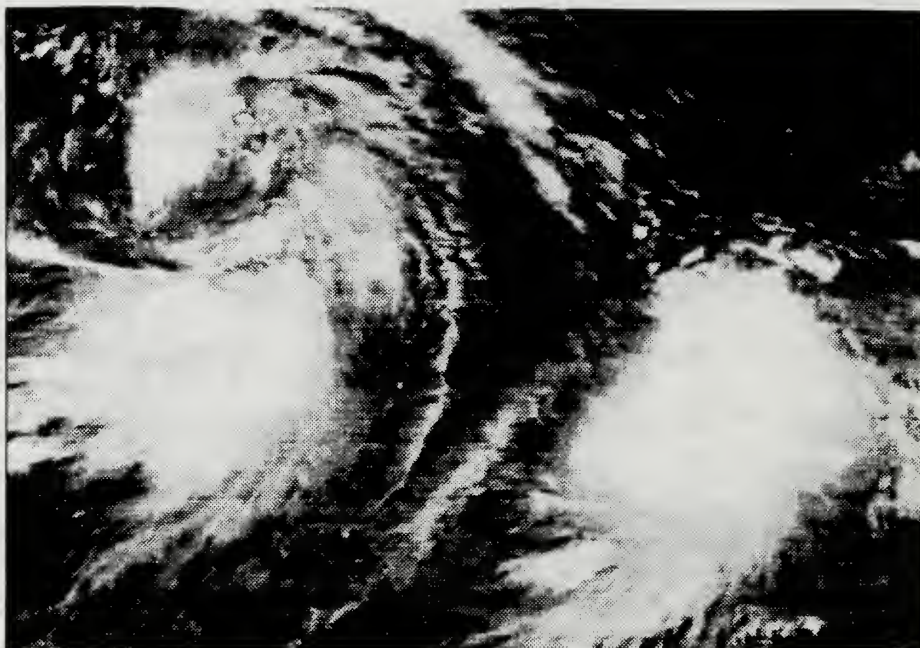


Figure 39. IR satellite imagery for 0330 UTC 25 August 1992 showing the outflow from TD Polly (left side) meeting the outflow from TS Omar (right side) over a relatively cloud-free area between the storms.

that the outflows from Polly and Omar were meeting closer to TS Omar. Subsidence would presumably occur where the two flows met and would have assisted in building the intermediate ridge. According to JTWC, this mid-level ridging associated with the upper-level subsidence tended to block the westward motion of Omar (ATCR 1992). The subtropical ridge and the monsoon trough maintained their positions and the southwest monsoon continued to feed both storms.

At low levels, Omar is in a similar location to that of the cyclone (Fig. 12) that trails the anticyclone in a Rossby wave train generated by a monsoon gyre. This inflow of energy could result in increased low-level convergence to Omar, which

would result in increased latent heat release necessary for maintenance and intensification of Omar.

The 200 mb analysis (Fig. 38b) showed that the flow from the anticyclone associated with the monsoon gyre and TD Polly was increasing. The TUTT cell to the northeast had also increased, which strengthened the flow that impinged on the upper-level anticyclone over TS Omar. This is seen as a bow-wave effect in Fig. 38b, and TS Omar's outflow was constricted to the south to southwest.

The vertical wind shear over Omar remained moderate to strong during the tropical storm period and this is confirmed by the soundings at Guam, with magnitudes that are somewhat lower (Fig. 32). The distance of Omar to Guam decreased from 8 deg. lat. at 00 UTC 25 August to 4 deg. lat. at 00 UTC 27 August. The quick decrease in magnitude at Guam at the end of the period occurred because a northeast flow at low levels was underneath an upper-level northeast flow. The intensity (maximum velocity), speed of movement, and magnitude of wind shear during the TS stage are compared in Fig. 33. TS Omar started to have a slower speed of movement 6 h after the onset of the stronger vertical wind shear, and it reached a minimum translation of 4 kt at 18 UTC 26 August. Similar to the TD stage, the moderate vertical wind shear did not prevent intensification during the TS stage. Perhaps the intensity changed more slowly around 00 UTC 26 August, but these values may have been due to inaccuracies in the satellite

interpretation. Whereas the increased vertical wind shear appeared to play a role in reducing the speed of movement, it only slowed the intensification.

The EFC (Fig. 34) remained negative within 300 km of the vortex during the entire stage. This was probably due to the upper-level anticyclone over Omar.

Based on satellite imagery, TD Polly had a larger horizontal circulation than TS Omar. However, Polly still did not develop a core of central convection. The deep convection associated with Polly was found around the edge of its circulation. Large areas of deep convection were also located within the monsoon gyre between Polly and Omar. Generally, Omar appeared to be better organized than Polly. The first visual effect of the impinging vertical wind shear was to decrease the size of Omar's circulation. On 25 August, the central convective area contracted into a tight spiral, and it continued as a smaller circulation for the remainder of its life cycle. The strong upper-level flow impinging on TS Omar from the north in conjunction with the daytime warming of cloud tops caused partial exposure of the mid-level vortex (Fig. 40) from 0030-0730 UTC 26 August. The deep convection was located over the southwest portion of the LLCC. Thus, the latent heat release would still be circulated around the vortex, with possible forced descent near the center assisting in intensifying Omar as in the model (Fig. 17b) described in Chapter IV. Animated IR satellite imagery showed that the

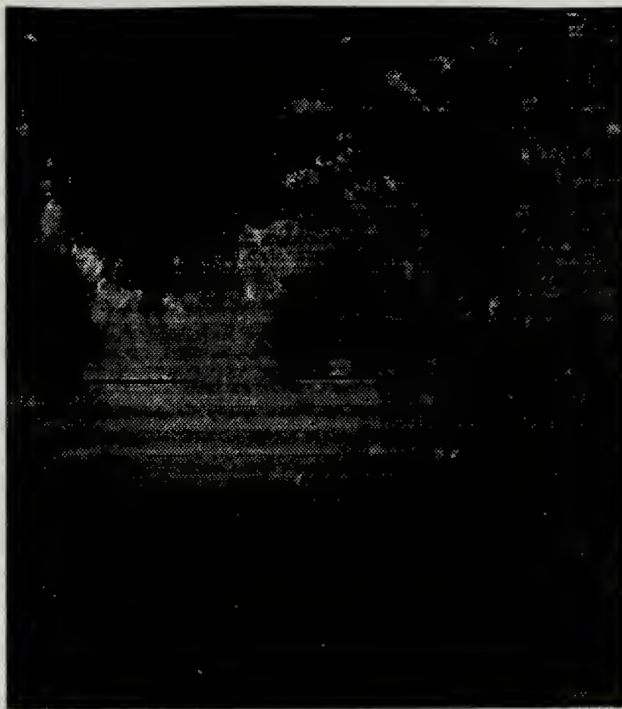


Figure 40. Visible satellite imagery for 0530 UTC 26 August showing the partially exposed mid-level vortex of TS Omar with the deepest convection located over the southwest portion of the vortex.

vortex recovered during the nighttime hours, which was seen in the increasing area of cloud top temperatures less than -85°C around the center. Although Polly was not well organized, the outflow from Polly and the upper-level anticyclone associated with the monsoon gyre were able to produce strong vertical wind shear similar to that generated by the leading typhoons in the Steve and Zola cases.

Although the strong vertical shear might have been expected to decouple Typhoon Omar's upper- and lower-level circulations, the storm remained vertically coherent against the shear. As in the cases of Steve and Zola, the location of

the deepest convection on the southwest part of the partially exposed mid-level vortex during the shear episode assisted in system maintenance by circulating latent heat released from convection to circulate around the core and allow system maintenance vice ventilation. The inertial stability of the inner core at low levels in the tropical storm reduces the effects of the environment at low levels. This should increase the ability of the tropical storm to "fight off" the effects of vertical wind shear at upper levels. Thus, only the mid-level vortex was exposed.

D. TYPHOON STAGE (06 UTC 27 AUGUST TO 00 UTC 28 AUGUST)

As TS Omar drifted northwestward, it slowly intensified and was upgraded to a typhoon at 06 UTC 27 August. The separation distance between the two systems increased to over 22 deg. lat. as TS Polly tracked west-northwest at 8 kt and Typhoon Omar moved northwest at 4-6 kt (Fig. 30). As the vertical wind shear decreased, intensity increased, and Typhoon Omar's speed of movement increased (Fig. 33). Omar underwent rapid intensification starting from 18 UTC 27 August and continuing for 12 to 18 h (ATCR 1992). The EFC (Fig. 36) became positive during after 12 UTC 27 August, which corresponded well to the period of rapid intensification. The positive EFC is due to the movement of an upper-level midlatitude trough moving eastward north of Omar.

Typhoon Omar began tracking west-northwest at 18 UTC 27 August and it began to accelerate toward Guam. According to JTWC (ATCR 1992), Typhoon Omar passed over Guam with destructive winds in excess of 50 kt occurring on the island for 16 h. Omar caused an estimated \$457 million of damage.

E. SUMMARY

When the upper-level outflow from Polly combined with a strong TUTT cell to the east, strong vertical wind shear impinged on Omar, which slowed Omar's rate of intensification. However, Omar maintained its intensity against the shear and even continued to slowly intensify. The Rossby wave dispersion of the monsoon gyre caused the development of a mid-level anticyclone, which forced Omar to slow down. Subsidence between Polly and Omar assisted in building the anticyclone. When the distance between the storms increased, Omar's translation speed and rate of intensification increased.

While Omar was enduring moderate to strong vertical wind shear, the location of the deepest convection was in a pattern similar to Steve and Zola. The coldest cloud tops were on the opposite side of the system center from the strong shear. When the mid-level vortex was exposed, the deep convection was over the southwestern part of the vortex. The models for maintaining the system discussed in the Steve case (Fig. 17) are valid here. The Rossby wave train hypothesis was not a

part of the formation of Omar but the development of a Rossby wave train by the monsoon gyre, in which Polly was embedded, could have assisted in the maintenance and intensification of Omar. At low levels, Omar is in a similar location to that of the cyclone that trails the Rossby wave train anticyclone (Fig. 12). This energy dispersion into Omar could have increased low-level convergence, and increased latent heat release in convection necessary for maintenance and intensification.

VII. CONCLUSIONS

A. SUMMARY AND DISCUSSION

The three cases document the development and/or intensification of a TC under moderate to strong shear that exceeded threshold values while in the lee of another TC. Data resources used for the three cases included hand-drawn analyses, multi-quadric analyses, and TCM-90 analyses. There was good agreement in all three cases between the hand analyses and the computer-generated analyses. The hand analyses occasionally contained more mesoscale features that did not appear in the computer-generated analyses. However, the flow patterns over the developing systems and the location of major synoptic features were very similar. Because the multi-quadric analyses were generated using NOGAPS as a first-guess field, the multi-quadric analyses were very similar to the NOGAPS fields with some minor changes in wind direction and speed but no changes in locations of major features. The computer-generated analyses did not detect a low- or upper-level circulation for TC Steve, TC Zola, and TC Omar in the disturbance and depression stages. A low-level circulation was detected in the tropical storm stage for each case. The calculations of vertical wind shear, relative vorticity, and

convergence would represent the contributions of the synoptic environment in which the TCs developed.

The tracks and intensities of each TC were generated at JTWC. JTWC uses the empirical Dvorak technique as a first guess in the intensity forecast and then modifies this estimate after evaluating the climatology and synoptic situation (ATCR 1990). The post-season (best-track) analyses of storm intensities relies heavily on the empirically derived central pressure-maximum wind relationship (Dvorak 1984). Comparisons of the operational satellite intensity estimates with best-track estimates indicate an average difference from the best-track maximum winds of 3 kt in the western North Pacific region (Dvorak 1984). However, this difference may be too small due to an over-reliance on the satellite estimates in best-track evaluations. The intensities for TC Zola and TC Omar are the best-track calculations while the intensities for TC Steve were the operational estimates. Although the accuracy of the best-track intensities are better for TC Zola and TC Omar, the intensities for TC Steve should be fairly accurate and representative of the development and intensification of the TC.

TC Steve and TC Zola developed within monsoon trough circulations containing the leading TCs. Low-level wind surges within the monsoonal flow initially contributed to the development of TC Steve and TC Zola. TC Steve formed northeast of the low-level equatorial anticyclone associated

with the Rossby dispersion pattern of TC Robyn and large cross-equatorial flow into the monsoon trough. TC Zola formed on the eastern edge of the monsoon gyre that also contained TC Yancy and another low pressure center to the southwest. TC Omar formed prior to the development of its leading TC, with both systems forming in the realignment of the monsoon trough into its normal location within the western North Pacific. TUTT-associated divergence contributed to the development of TC Steve and TC Zola.

TC Steve and TC Zola developed under moderate to strong shear due to the large-scale environment. The outflow from both leading TCs was constricted on the eastern side, and this allowed TC Steve and TC Zola to form close to the leading system and outside of the Rossby dispersion patterns. TC Omar formed under low vertical shear, and the episode with moderate to strong shear occurred during the tropical storm stage. The vertical shear was time dependent due to the complex interaction with the leading TC outflow, adjacent TUTT, and large-scale environment. The leading TC was not the primary contributor to the shear during any of the three cases, but rather the upper-level anticyclone associated with the low-level monsoon gyre in combination with the TUTT provided the strong upper-level impinging flow.

The intensification of the three TCs was not correlated with EFC. The EFC calculations for TC Steve and TC Omar are less accurate than for TC Zola due to the availability of high

resolution TCM-90 analyses for TC Zola. The accuracy of these EFC values is somewhat uncertain since the number of observations entered into these computer-generated analyses is small, and the analyses generally represent only synoptic-scale features.

The hypothesis that a new storm cannot develop at separation distances less than 9 deg. lat. due to strong vertical wind shear generated by the pre-existing TC was invalidated by TC Zola but not by TC Steve. TC Zola formed at a distance of 7 deg. lat. from TC Yancy while TC Steve formed at 11.9 deg. lat. from TC Robyn. The upper-level outflow from TC Yancy was constrained on the eastern side, which allowed TC Zola to form closer than the Briegel (1993) minimum separation distance.

Analysis of high resolution satellite imagery indicated the diurnal variability in the strength of convection and outflow against the impinging flow, which led to a fully exposed, partially exposed, or covered mid- to lower-tropospheric cyclonic circulation. The deep convection was located on the edges or southwestern section of the exposed vortex. The forced descent that is created when the outflow meets the impinging flow can occur over the center or edge of the exposed circulation, which may provide additional heat to maintain the warm core (Fig. 17).

For all three cases, the TC maintained and intensified its circulation while under the moderate to strong shear. Special

characteristics of the monsoon trough circulation evidently create and sustain the TC circulation against the tendency for the vertical shear to ventilate the vertical thermal and convective structure. Further cases are required to document the conditions in which vertical wind shear can or cannot disrupt the development or intensification of TCs.

B. FUTURE INVESTIGATIONS

This study has provided evidence that TCs can develop and intensify under moderate to strong vertical wind shear. Although forecast thumb rules state that trailing TCs usually form at a separation distance of 1000 to 2000 km, TC Zola formed within 780 km of TC Yancy. The separation distance appears to not be a critical factor during the disturbance stage. The results of this study clearly contradict the TC development rules requiring minimum vertical wind shear. This makes it more difficult for a forecaster to eliminate areas for the formation of TCs due to the presence of moderate to strong vertical wind shear.

These case studies indicate some possible mechanisms that may maintain and intensify the TCs under the moderate to strong shear. However, a number of aspects of TC development and/or intensification must be addressed.

- . Storms that develop under exposure to moderate to strong vertical wind shear tend to be smaller; and
- . Exposure to shear slows/modifies the track of the TC presumably due to asymmetric distribution of heating.

Finally, the conceptual models of partially- or fully-exposed low-level circulations raise some challenges to modelling the distribution of heating in these developing and intensifying TCs.

LIST OF REFERENCES

- ATCR, 1990: Annual tropical cyclone report. U.S. Naval Oceanography Command Center, COMNAVMARIANAS, Box 12, FPO AP 96540-0051, 185 pp.
- ATCR, 1992: Annual tropical cyclone report. U.S. Naval Oceanography Command Center, COMNAVMARIANAS, Box 12, FPO AP 96540-0051, 269 pp.
- Bartels, D.L., and R.A. Maddox, 1991: Midlevel cyclonic vortices generated by mesoscale convective systems. **Mon. Wea. Rev.**, **119**, 104-118.
- Briegel, L.M., 1993: The role of large-scale flow in tropical cyclogenesis in the western Pacific Ocean. Masters Thesis, Pennsylvania State University, University Park, PA, 110 pp.
- Carr, L.E., and R.L. Elsberry, 1994: Monsoonal interactions leading to sudden tropical cyclone track changes (submitted).
- Charney, J.G., and A. Eliassen, 1964: On the growth of the hurricane depression. **J. Atmos. Sci.**, **36**, 2617-2630.
- Challa, M., and R.L. Pfeffer, 1990: Formation of Atlantic hurricanes from cloud clusters and depressions. **J. Atmos. Sci.**, **47**, 908-927.
- Chen, L., and W.M. Gray, 1986: Global view of the upper outflow patterns associated with tropical cyclone intensity change during FGGE. **Atmos. Sci. Paper No. 392**, Colorado State University, Ft. Collins, CO 80523, 126 pp.
- DeMaria, M., J.J. Baik, and J. Kaplan, 1993: Upper-level eddy angular momentum fluxes and tropical cyclone intensity change. **J. Atmos. Sci.**, **50**, 1133-1148.
- Dvorak, V.F., 1984: Tropical cyclone intensity analysis using satellite data. **NOAA Tech. Rpt. NESDIS 11**, U.S. Dept. of Commerce, Washington DC, 47 pp.
- Elsberry, R.L., 1987: Tropical cyclone motion. Chap. 4, **A Global View of Tropical Cyclones**, R.L. Elsberry (Ed.), Office of Naval Research, Arlington, VA 22217, 91-127.

- Elsberry, R.L., B.C. Diehl, J.C.-L. Chan, P.A. Harr, G.J. Holland, M. Lander, T. Neta, and D. Thom, 1990: ONR tropical cyclone motion research initiative: field experiment summary. Tech. Rpt. NPS-MR-91-001, Naval Postgraduate School, Monterey, CA 93943, 107 pp.
- Emanuel, K.A., 1991: A scheme for representing cumulus convection in large-scale models. **J. Atmos. Sci.**, **48**, 2313-2335.
- Evans, J.L., 1993: Sensitivity of tropical cyclone intensity to sea surface temperature. **J. Climate**, **6**, 1133-1140.
- Frank, W.M., 1982: Large-scale characteristics of tropical cyclones. **Mon. Wea. Rev.**, **110**, 572-586.
- Frank, W.M., 1987: Tropical cyclone formation. Chap. 3, **A Global View of Tropical Cyclones**, R.L. Elsberry (Ed.), Office of Naval Research, Arlington, VA 22217, 53-90.
- Gray, W.M., 1968: Global view of the origin of tropical disturbances and storms. **Mon. Wea. Rev.**, **96**, 669-700.
- Gray, W.M., 1975: Tropical cyclone genesis. Dept. of Atmos. Sci. Paper No. 232, Colorado State University, Ft. Collins, CO, 121 pp.
- Gray, W.M., 1979: Hurricanes: their formation, structure and likely role in the tropical circulation. **Meteorology over the Tropical Oceans**, D.B. Shaw (Ed.), Royal Meteorology Society, 115-218.
- Hane, C.E., 1986: Extratropical squall lines and rainbands. **Mesoscale Meteorology and Forecasting**, P. Ray (Ed.), Amer. Meteor. Soc., Boston MA 02108, 359-388.
- Hogan, T., and T. Rosmond, 1991: The description of the Navy operational global atmospheric prediction system's spectral forecast model. **Mon. Wea. Rev.**, **119**, 1786-1815.
- Lander, M.A., 1993: The northward-displaced, self-sustaining solitary (NSS) monsoon gyre (Submitted).
- McBride, J.L., and R. Zehr, 1981: Observational analysis of tropical cyclone formation: Part II. Comparison of non-developing versus developing systems. **J. Atmos. Sci.**, **38**, 1132-1151.
- Menard, R.D., and J.M. Fritsch, 1989: A mesoscale convective complex-generated inertially stable warm core vortex. **Mon. Wea. Rev.**, **117**, 1237-1261.

- Molinari, J., and D. Vollaro, 1989: External influences on hurricane intensity. Part I: Outflow layer eddy-angular momentum fluxes. **J. Atmos. Sci.**, **46**, 1093-1105.
- Molinari, J., and D. Vollaro, 1990: External influences on hurricane intensity. Part II: Vertical structure and response of the hurricane vortex. **J. Atmos. Sci.**, **47**, 1902-1918.
- Nuss, W.A., and D.W. Titley, 1994: Use of Multiquadric interpolation for meteorological objective analysis. **Mon. Wea. Rev.** (in press).
- NWS, 1993: The effects of vertical speed shear on thunderstorm growth. **Western Region Tech. Attachment No. 93-28**, National Weather Service, Salt Lake City, UT, 5 pp.
- Ooyama, K., 1963: A dynamical model for the study of tropical cyclone development. 43rd Annual Meeting of the American Meteorological Society, January 21-24, New York, 26 pp.
- Pfeffer, R.L., and M. Challa, 1981: A numerical study of the role of eddy fluxes of momentum in the development of Atlantic hurricanes. **J. Atmos. Sci.**, **38**, 2393-2398.
- Rao, P.K., S.J. Holmes, R.K. Anderson, J.S. Winston, and P.E. Lehr, 1990: Weather satellites: systems, data, and environmental applications. American Meteorological Society, Boston, MA 02108.
- Rotunno, R., and K.A. Emanuel, 1987: An air-sea interaction theory for tropical cyclones. **J. Atmos. Sci.**, **44**, 542-560.
- Sadler, J.C., 1976: Tropical cyclone initiation by the tropical upper tropospheric trough. Tech. Paper No. 2-76, Navy Environmental Prediction Research Facility, Monterey, CA, 103 pp.
- Sadler, J.C., 1978: Mid-season typhoon development and intensity changes and the tropical upper tropospheric trough. **Mon. Wea. Rev.**, **106**, 1137-1152.
- Simpson, R.H., 1971: Decision process in hurricane forecasting. Tech. Memo. SR 53, National Weather Service, Salt Lake City, UT, 35 pp.

Tuleya, R.E., and Y. Kurihara, 1981: A numerical study on the effects of environmental flow on tropical storm genesis. **Mon. Wea. Rev.**, **109**, 2487-2506.

Zehr, R.M., 1992: Tropical cyclogenesis in the western North Pacific. NOAA Tech. Rpt. NESDIS 61, U.S. Dept. of Commerce, Washington DC, 181 pp.

INITIAL DISTRIBUTION LIST

	No. Copies
1. Defense Technical Information Center Cameron Station Alexandria VA 22304-6145	2
2. Librarian Code 52 Naval Postgraduate School 411 Dyer Rd Rm 104 Monterey CA 93943-5101	2
3. Oceanography Department Code OC/CO Naval Postgraduate School 833 Dyer Rd Rm 331 Monterey CA 93943-5122	1
4. Meteorology Department Code MR/HY Naval Postgraduate School 589 Dyer Rd Rm 252 Monterey CA 93943-5114	1
5. Dr. R.L. Elsberry Code MR/Es Naval Postgraduate School 589 Dyer Rd Rm 252 Monterey CA 93943-5114	2
6. Dr. P.A. Harr Code MR/Hr Naval Postgraduate School 589 Dyer Rd RM 252 Monterey CA 93943-5114	1
7. Lt. Debra K. Smith, USN 433 Casa Verde Way Apt 231 Monterey CA 93940	1
8. Commanding Officer Fleet Numerical Meteorology and Oceanography Center 7 Grace Hopper Ave Stop 4 Monterey CA 93943-0120	1

9. Chief of Naval Research
800 N. Quincy Street
Arlington VA 22217
10. Commanding Officer
Naval Pacific Meteorology and Oceanography Center
COMNAVMARIANAS Box 12
FPO AP 96540-0051
11. Air Weather Service Technical Library
Scott AFB, IL 62225-5008
12. Cdr. L. Carr III
Code MR/Cr
Naval Postgraduate School
589 Dyer Rd Rm 252
Monterey CA 93943-5114

DUDLEY KNOX LIBRARY
NAVAL POSTGRADUATE SCHOOL
MCS 43-5101



GAYLORD S

DUDLEY KNOX LIBRARY



3 2768 00307037 6